# **TEKTONIKA**



## The drivers of Lower Crustal Earthquakes Along Magma-Poor Portions of the East African Rift

Luke Wedmore  $\bigcirc^1$ , Jack Williams  $\bigcirc^{*2}$ , Juliet Biggs  $\bigcirc^1$ , Ake Fagereng  $\bigcirc^3$ , Joanna M. Holmgren  $\bigcirc^{1,4}$ , Maximilian J. Werner  $\bigcirc^1$ , Felix Mphepo<sup>5</sup>

<sup>1</sup>School of Earth Sciences, University of Bristol, Bristol, UK | <sup>2</sup>Department of Geology, University of Otago, Dunedin, New Zealand | <sup>3</sup>School of Earth and Environmental Sciences, Cardiff University, Cardiff, UK | <sup>4</sup>NORSAR, Kjeller, Norway | <sup>5</sup>Geological Survey Department, Malawi

Abstract Deep earthquakes along magma-poor sections of the East African Rift System (EARS) challenge our understanding of the controls on seismogenic thickness because they occur at greater depths and higher temperatures than the frictional-viscous transition zone in typical continental crust. Using a recently published catalogue of relocated earthquakes in southeastern Africa, we demonstrate that seismicity occurs down to the  $\sim 40$  km deep Moho throughout the magma-poor southern EARS. We then explore the mechanisms that can account for this deep seismicity by combining 1D lithospheric strength profiles with available regional measurements of Moho thickness, the ratio of the crust's P- and S-wave velocities  $(V_P/V_S)$ , and heat flow. As suggested by previous studies, we find that a mafic lower crustal composition, lower geothermal gradient, and/or high pore fluid pressure can locally facilitate the observed deep seismicity. However, there are sections of the southern EARS where the lower crust is felsic, dry, and warm, and in these cases, we propose that the embrittlement of the lower crust is best explained by strain localisation in space and time. This strain localisation could occur because fault and shear zones in magma-poor sections of the EARS are unusually narrow, or because strain is localised in space and time following large magnitude earthquakes.

Executive Editor:
Robin Lacassin
Associate Editor:
Guillaume Duclaux
Technical Editor:
Mohamed Gouiza

Reviewers:
Ameha Muluneh
Folarin Kolawole
Rasheed Ajala

Submitted:
1 July 2024
 Accepted:
4 June 2025
 Published:
27 July 2025

#### 1 Introduction

Seismicity along southern portions of the East African Rift System (EARS) presents a challenge to our understanding of the forces controlling plate tectonics and the rheology of the lithosphere (Buck, 2004). Neither far-field boundary forces nor internal body forces are thought to be sufficient to overcome the strength of intact lithosphere in the region, which is old, cold and thus strong (Fagereng et al., 2024; Kendall and Lithgow-Bertelloni, 2016; Rajaonarison et al., 2021; Stamps et al., 2014). However, teleseismic (e.g., Craig and Jackson, 2021) and local earthquake (Ebinger et al., 2019; Lavayssière et al., 2019; Stevens et al., 2021) studies conclusively show that seismicity occurs down to approximately 40 km depth along the Western Branch of the EARS. This implies that earthquakes are occurring at temperatures that are warmer than normally considered for the base of the frictional-viscous transition in a quartz-dominated continental crust (i.e.,  $>\sim 350$  °C). Thus, the thick, frictional seismogenic zone, if it is a stable feature, has the effect of strengthening the crust and making it harder to rift. Nonetheless, the western and southwestern branches of the EARS are actively accommodating strain (Stamps et al., 2021; Wedmore et al., 2021), have numerous active faults (Daly et al., 2020; Shillington et al., 2020; Wedmore et al., 2022; Williams et al., 2022a), and have recorded moderate to large magnitude (M 6-7.3) earthquakes over the past century (Ambraseys and Adams, 1992; Meghraoui and the IGCP-601 Working Group, 2016).

Several non-mutually-exclusive mechanisms have been invoked to contribute to lower crustal seismicity along the EARS: (1) the presence of magmatic and/or volatile rich fluids in the lower crust (Ajala et al., 2024; Gardonio et al., 2018; Lavayssière et al., 2019; Paulssen et al., 2022), (2) localised strain within a laterally heterogeneous lower crust and/or upper mantle (Fagereng, 2013; Kolawole et al., 2017; Moorkamp et al., 2019; Wedmore et al., 2020a) (3) a relatively low geothermal gradient (Craig and Jackson, 2021; Nyblade and Langston, 1995), and (4) compositional variation in the lower crust, such as a mafic layer (Hellebrekers et al., 2019; Nyblade and Langston, 1995; Shudofsky et al., 1987). These mechanisms may be interconnected, because fluid-related processes -including initiation of partial melting- require a fluid source external to the currently dry lower crust, and initiation of fluid flow needs deformation to generate permeability (Fagereng et al., 2024). Understanding when and where these various mechanisms drive lower

crustal seismicity along the southern EARS is not only important for understanding lithospheric rheology, but it can also reduce seismic hazard modelling uncertainties for this region (*Gounon et al.*, 2021; *Williams et al.*, 2023).

Here we first analyse a new seismicity catalogue for the southern EARS that systematically relocated earthquakes using data from publicly available seismic campaigns and permanent seismic networks in this region (section 3; Holmgren et al., 2023), and place these earthquake locations in the context of existing seismic determinations of Moho depth and crustal velocity. In section 4, we then use 1-D lithospheric strength profiles to review the mechanisms that can explain the distribution and potential causes of the deep seismicity in the southern EARS, and test these profiles against observations from the Holmgren et al. (2023) catalogue.

## 2 Geologic and tectonic setting of the southern East Africa Rift System

In recent years, it has been suggested that rather than a single EARS plate boundary in southeastern Africa, regional strain is accommodated within a network of deforming zones that separate Archean cratons and host most of this region's seismicity (Daly et al., 2020; Wedmore et al., 2021). For example, in southern Tanzania, the Western Branch bifurcates into the Southwestern Branch, which extends into Zambia, Botswana, and Namibia, and includes the Luangwa and Okavango rifts (Line B-B' in Figure 1a; Daly et al., 2020; Grant et al., 2024; Kinabo et al., 2008; Wanke, 2005; Wedmore et al., 2022). Rifting in the Western Branch initiated by the late Oligocene  $\sim 25$  Ma (Roberts et al., 2012), and possibly as early as the Eocene (Jess et al., 2020), whereas rift initiation along the Southwestern Branch is unclear, with periods of regional cooling between 38-22 Ma and 5-3 Ma (Daly et al., 2020). Extension rates decrease from north to south along both the western  $(2.7\text{-}0.4 \text{ mm } yr^{-1})$  and southwestern (0.7-0.4mm  $yr^{-1}$ ) branches (Saria et al., 2014; Wedmore et al., 2021).

Two further southern EARS branches, both of which follow the boundaries of the Zimbabwe craton, have also been proposed. The San-Angoni boundary (SAB) consists of a series of faults and basins that run along the northern edge of the Zimbabwe craton between southern Malawi and southern Zambia (Line D-D' in Figure 1a; Daly et al., 2020; Mackintosh et al., 2019), although there is not yet sufficient geodetic evidence to support the existence of this as an active branch (Wedmore et al., 2021). To the south of the Zimbabwe Craton lies the granulite facies Neoarchaen-Paleoproterozoic Limpopo-Sashe orogenic belt (LSB). Notably, the 2017  $M_W$  6.5 Botswana Earthquake was hosted within the LSB (Gardonio et al., 2018; Kolawole et al., 2017; Midzi et al., 2018; Paulssen et al., 2022), and although proposed by some to be an intraplate event (Gardonio et al., 2018), the Botswana Earthquake may instead be part of a wider zone of active faulting and seismicity that runs between the Kaapvaal and Zimbabwe cratons into Mozambique (Line C-C' in Figure 1a; Meghraoui and the IGCP-601 Working Group, 2016; Midzi et al., 2018; Paulssen et al., 2022). In contrast to the Eastern Branch of the EARS, which is characterised by extensive magmatic activity (Biggs et al., 2021), volcanism in these southern EARS branches is limited to four isolated provinces along the Western Branch (Toro-Ankole, Virunga, South Kivu, and Rungwe provinces; Ebinger, 1989).

## 3 Insights into southern East African Rift System Earthquakes from Instrumental Catalogues

#### 3.1 Earthquake Catalogues

Many areas now have dense networks of seismometers that enable earthquake catalogues with a magnitude of completeness down to  $M_W$  3.0, e.g. in Italy, Greece, Japan, USA, New Zealand (Petersen et al., 2011). Along the southern parts of the EARS, there are only 62 permanent seismic stations covering an area of  ${\sim}6$ million  $km^2$ , representing an average of 0.01 stations per  $1000 \ km^2$ , compared with the USA, which has 1.3 stations per 1000  $km^2$  (12,679 stations in  $\sim$ 9.5 million  $km^2$ ; data from IRIS (https://www.iris.edu/) and excluding Raspberry Shake stations). Consequently, the magnitude of completeness in southern Africa catalogues is relatively high  $(M_W 4.5 - 5; Hodge et al.,$ 2015; Poggi et al., 2017), with the detection of smaller magnitude earthquakes often reliant on temporary local seismic networks (Ebinger et al., 2019; Lavayssière et al., 2019; Stevens et al., 2021). In addition, a combination of East Africa's short instrumental period (<100 years) and locked low-slip rate faults means that the moment release indicated by earthquake catalogues represents only a small proportion of the moment rate indicated by geodesy (Ebinger et al., 2019; Williams et al., 2023); nevertheless, that is not to say that East Africa's incomplete record of seismicity cannot be used to investigate the rheology of its crust.

Here, we focus on earthquakes catalogued by *Holmgren* et al. (2023) (henceforth referred to as H23) who compiled publicly available records of 882 M earthquakes that occurred in and around the southern EARS between 1994-2022 and had epicentral distances < 300 km. We then filtered these events by considering: (1) events located south of 4.5°S, which with the exception of the Rungwe Volcanic Province, means they occurred within non-volcanic sections of the EARS, and (2) were relocated in NonLinLoc using P- and S-wave phases that were manually picked using publicly available waveform data and the Ebinger et al. (2019) regional velocity model. In total, this leaves 224 earthquakes, and it is these events that form the basis of our analysis. In addition, we associate events with each southern EARS rift branch by searching for those that are located within 75 km of the rift axis as shown in Figure 1; this is broadly

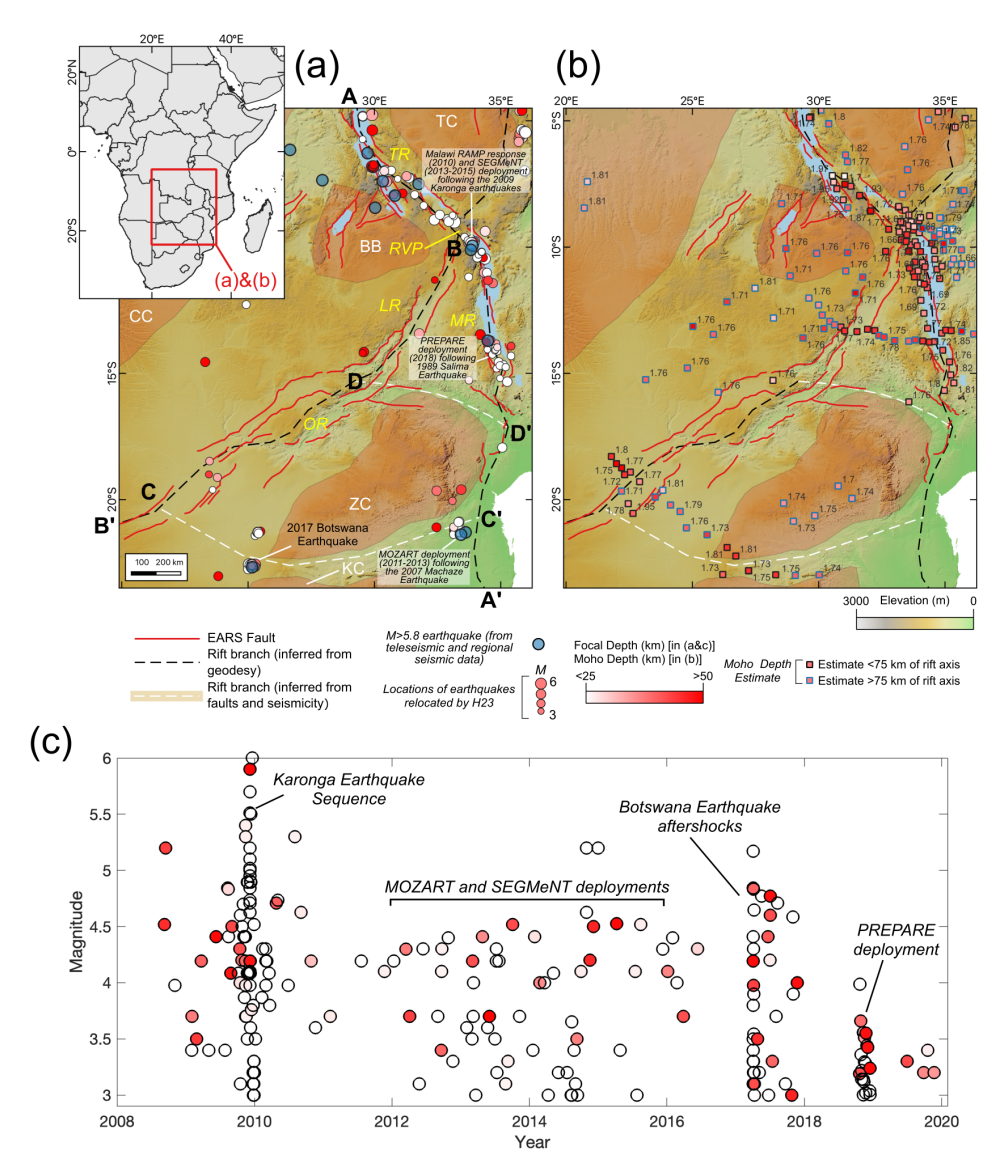


Figure 1 – (a) Seismicity in southeastern Africa from events relocated by  $Holmgren\ et\ al.\ (2023)\ (H23)\ and\ M_W\ 5.8\ earthquakes$  between 1980-2020 that were located from teleseismic and regional waveforms by  $Craig\ et\ al.\ (2011)\ and\ Craig\ and\ Jackson\ (2021)$ . Lines A-A' is the Western Branch, B-B' is the Southwestern Branch, C-C' is the Kaapvaal-Zimbabwe boundary, and D-D' is the San-Angoni Boundary. BB = Bangweulu Block, CC = Congo Craton, KC = Kaapvaal Craton, TC = Tanzania Craton, ZC = Zimbabwe Craton, TR = Tanganyika Rift, MR = Malawi Rift, LR = Luangwa Rift, OR = Okavango Rift, RVP = Rungwe Volcanic Province. Mapped faults from  $Daly\ et\ al.\ (2020)\ and\ Hodge\ et\ al.\ (2018)$ . Inset, location map for (a) & (b). (b) Map indicating Moho depths estimates for the area shown in (a) from receiver functions (see text for references). The values reported next to the Moho depths are the station's  $V_P/V_S$  ratio estimate. (c) Temporal distribution of events in the H23 catalogue. Where available, the reported magnitudes in (a) and (c) are  $M_W$ , as compiled by H23. Otherwise, they are the magnitude (Mb or Ml) originally reported for the event.

consistent with the 50-150 km rift widths indicated by southern EARS active fault maps (*Grant et al.*, 2024; *Muirhead et al.*, 2019; *Wedmore et al.*, 2022; *Williams et al.*, 2022a). This analysis is not conducted for the San-Angoni boundary, as there are no earthquakes < 75 km of this branch within the H23 relocated catalogue.

# 3.2 Spatial-temporal Distribution of Seismicity

The earthquakes relocated by H23 are mostly concentrated along the Western Branch, but seismicity is also observed along the Southwestern Branch, and the Kaapvaal-Zimbabwe craton boundary (Figures 1a and 2, Table 1). In total, we find that just 37/224 (17%) of

the events in the H23 relocated catalogue are located >75 km from a rift axis (Table 1); this increases to 88/224 (39%) of events if we use a stricter criterion of 35 km to filter rift events. We note, however, that this result also reflects the relatively enhanced seismometer coverage along the rift ( $Holmgren\ et\ al.$ , 2023).

Events in the H23 catalogue are also heterogeneously distributed in time (Figure 1c). This spatial-temporal clustering mainly reflects aftershock sequences, with 68 of the 224 earthquakes located within 25 km, and subsequent to, one of the 13  $M_W$  5.8 earthquake that occurred in this region between 1980-2020 (using the catalogues from  $Craig\ et\ al.\ (2011)$  and  $Craig\ and\ Jackson\ (2021)$ , Figures 1a and 3). In part this reflects that aftershock sequences in southeastern Africa were

Table 1 – Summary statistics for earthquakes depths and crustal structure along branches of the southern EARS from the H23 relocated catalogue. Analysis is performed for earthquake locations and stations < 75 km from the branches as shown in Figure 1. Stable craton refers to earthquakes and stations > 75 km from a rift branch. Note: (1) events and receiver-function stations near branch junctions will be included in the analysis for > 1 branch, and (2) there are too few events to provide a  $d_{95}$  estimate for the Southwestern Branch.

| Region                    | Number of events in H23 catalogue | (km) | Number of receiver function observations | $\begin{array}{c} \textbf{Mean Moho Depth} \\ \textbf{(}\pm1\sigma,\mathbf{km)} \end{array}$ | $egin{array}{l} \mathbf{Mean} \; V_P/V_S \ (\pm 1\sigma, \; \mathbf{km}) \end{array}$ |
|---------------------------|-----------------------------------|------|--|--|---|
| Western Branch            | 125                               | 50.1 | 68                                       | $40.5 \pm 3.9$   | $1.76 \pm 0.08$   |
| Southwestern Branch       | 5                                 | n/a  | 20                                       | $42.6 \pm 3.4$   | $1.75 \pm 0.06$   |
| Kapvaal-Zimbabwe boundary | 52                                | 36.5 | 9  | $42.1 \pm 2.0$   | $1.78 \pm 0.07$   |
| Stable craton             | 37                                | 50.4 | 130                                      | $39.9 \pm 3.6$   | $1.75 \pm 0.04$   |

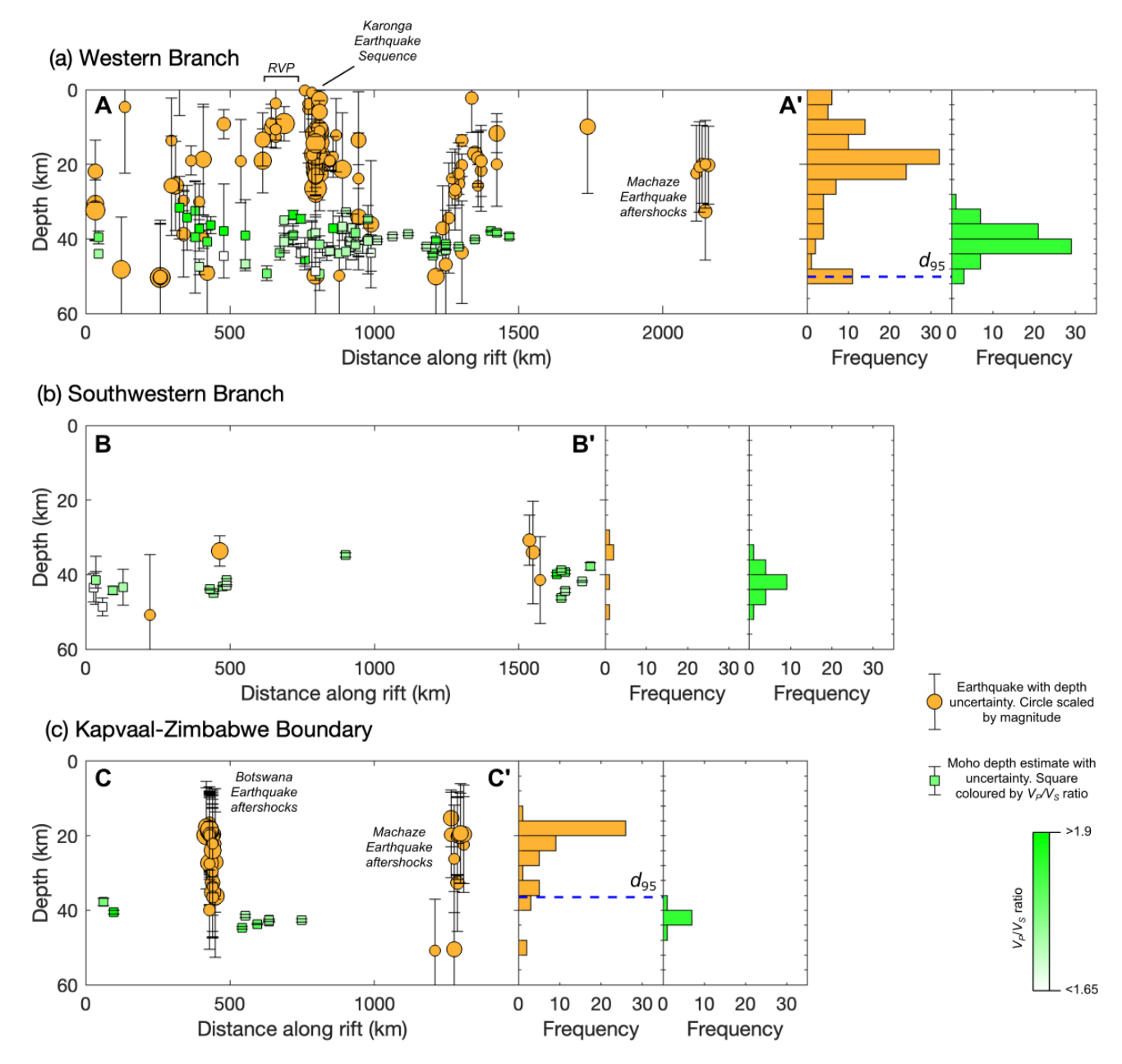


Figure 2 – Along rift profiles indicating the depth-distribution of earthquakes relocated by H23, crustal thickness, and bulk crustal  $V_P/V_S$  ratios in the southern EARS. Data is taken from earthquake locations and stations within 75 km of the rift axes as shown in Figure 1. Orange histograms are the depth distribution of events in 4 km depth bins, with the  $d_{95}$  value indicated by the blue dashed line. Green histograms show the distribution of receiver function estimates of Moho depth along each rift branch. RVP; Rungwe Volcanic Province.

the target of subsequent temporary seismic arrays, and so there was abundant local seismic data for H23 to relocate events (Figures 1-3); for example: the 2009 Karonga earthquake sequence (*Biggs et al.*, 2010; *Hamiel* 

et al., 2012; Macheyeki et al., 2015) and the Malawi RAMP Response and SEGMeNT deployment (Ebinger et al., 2019; Gaherty et al., 2019); the 1989  $M_W$  6.1 Salima Earthquake (Jackson and Blenkinsop, 1993)

and the PREPARE deployment (Stevens et al., 2021); and the 2006  $M_W$  7.0 Machaze earthquake (Copley et al., 2012; Lloyd et al., 2019) and the MOZART deployment (Fonseca et al., 2014). However, there are also some deployments that were not motivated by a large mainshock (e.g., the SAFARI deployment in the Luangwa Rift), and some  $M_W$  5.8+ earthquakes that were not the target of temporary seismic arrays (e.g. a  $M_W$  6.0 earthquake in Lake Tanganyika in 2005). Furthermore, some events in the H23 catalogue may be aftershocks of pre-1980 events. Notwithstanding the large ( $\sim < 50$  km) location uncertainties associated with historical seismicity in Africa (Ambraseys and Adams, 1992), possible examples of this include events in the vicinity of a M 5.9 earthquake in the Okavango Delta in 1952 and the 1910 M 7.3 Rukwa earthquake in southern Tanzania. Indeed, >100 year-long aftershock sequences in the low strain rate southern EARS would be consistent with global records that suggest relatively long aftershock durations in regions with low strain rates (Stein and Liu, 2009) and low surface heat-flow (Ben-Zion and Lyakhovsky, 2006).

### 3.3 Earthquake Depths

H23 found depth uncertainties ranging between  $\pm 20$ -30 km for the deepest earthquakes ( $\sim 50$  km), with the deepest well-constrained events ( $\pm 5$ -10 km) found at 35 km depth (Figure 2). So that our analysis of the maximum depth of seismicity in the southern EARS is not biased by poorly located hypocentres, we quantify variations in the maximum depth of seismicity using  $d_{95}$ , the depth above which 95% of earthquakes occur (Magistrale, 2001;  $Rolandone\ et\ al.$ , 2004). In this way, the depth uncertainties from individual events are smoothed out, and it allows us to systematically assess how the maximum depth of seismicity changes in both space and time.

We derive  $d_{95}$  estimates of 50 and 36 km along the Western Branch and the Kaapvaal-Zimbabwe boundary respectively (Figures 1 and 2, Table 1). There are too few earthquakes for us to provide a  $d_{95}$  estimate for the Southwestern Branch; however, the events that are associated with this branch have focal depths between 30-50 km (Figure 2b). One exception to the ubiquitous lower crustal earthquakes along the southern EARS may be present at the Rungwe Volcanic Province (RVP). Here there are few earthquakes with focal depths >25 km (Figure 2a), and although there are insufficient events in the H23 relocated catalogue to derive a RVP-specific  $d_{95}$ estimate, a thinner seismogenic crust is consistent with previous studies for this region (Ebinger et al., 2019). A locally reduced seismogenic crust thickness is also observed beneath the Western Branch's other volcanic provinces; 15-20 km at the South Kivu and Virunga volcanic provinces (Delvaux et al., 2017; Wood et al., 2017) and 15-25 km beneath the Toro-Ankole volcanic province (Lindenfeld et al., 2012a; Wedmore et al., 2024).

Our estimates of  $d_{95}$  from the H23 catalogue are consistent with previous regional studies, which indicate that southern EARS is hosted in crust that is seismogenic

to depths of 35-50 km (Craig and Jackson, 2021; Nyblade and Langston, 1995; Yang and Chen, 2010). However, we do not observe any clear change in the maximum depth of seismicity for events within or adjacent to the southern EARS (Table 1), or between the northern part of the Western Branch, hosted in  $\sim 120$  km thick lithosphere, and the Malawi Rift, hosted in  $\sim 160$  km thick lithosphere. It is therefore difficult to reconcile the deep crustal seismicity with a purely temperature-dependent model for the strength of the lithosphere (Craig and Jackson, 2021; Jackson et al., 2008). Considering the uncertainties associated with the focal depth estimates and estimates of crustal thickness, none of the relocated seismicity conclusively exceeds the Moho depth (Figure 2).

#### 3.4 Crustal Structure

We compile 233 estimates of Moho depth from receiver functions (see Supplementary Data) within and adjacent to the southern EARS (i.e., south of 4.5°S, Figures 1b and 2; Borrego et al., 2018; Hodgson et al., 2017; Kachingwe et al., 2015; Nair et al., 2006; Sun et al., 2021; Tugume et al., 2012; Yu et al., 2015). Along the Western Branch, most Moho depth estimates lie between 35-45 km depth (Figure 2a). The range in crustal thickness is greater along rift sections in Tanzania (32-48 km) compared with the measurements in Malawi ( $\sim$ 38-44 km; Figure 2a). Along the Southwestern Branch, the measurements of Moho depth are restricted to two basins. In the Luangwa Rift, crustal thickness varies between 35-45 km and there has been negligible crustal thinning across the rift (Sun et al., 2021). By contrast, the Moho is  $39.8 \pm 3.0$  km deep below the Okavango Rift and  $\sim 43 + 3$  km deep adjacent to the rift (Yu et al., 2015). Along the boundary between the Kaapvaal and Zimbabwe cratons, the Moho depth is between 38-45 km but no clear variation with distance is observed as measurements are only available from the western part of this boundary (Figures 1b and 2c). There are no clear differences in the depth to the Moho for sites within or adjacent to the rift (Figure 1, Table 1), indicating only minor, if any, crustal thinning along the southern EARS (Borrego et al., 2018; Hodgson et al., 2017; Hopper et al., 2020; Njinju et al., 2019a; Sun et al., 2021).

The ratio between P- and S-wave velocities  $(V_P/V_S)$  is often used as a proxy for the bulk rheology of the crust. Values between 1.7-1.8 usually indicate felsic to intermediate rocks, wheras higher values (>1.8) can indicate mafic rocks and/or the presence of partial melt or fluids within the crust (Ajala et al., 2024; Christensen, 1996). Along the Western Branch, there are 66 published estimates of  $V_P/V_S$ , and the median ratio is 1.74. Only 19 estimates exceed 1.8, and these are mainly located in the Tanganyika Rift (Figure 1b and 2a; Ajala et al., 2024; Hodgson et al., 2017) and RVP (Borrego et al., 2018). Along the Southwestern Branch,  $V_P/V_S$  ratios are locally elevated beneath the Okavango Rift (1.82  $\pm$  0.08; Yu et al., 2015) but are ~1.75 beneath the Luangwa Rift (Sun et al., 2021).

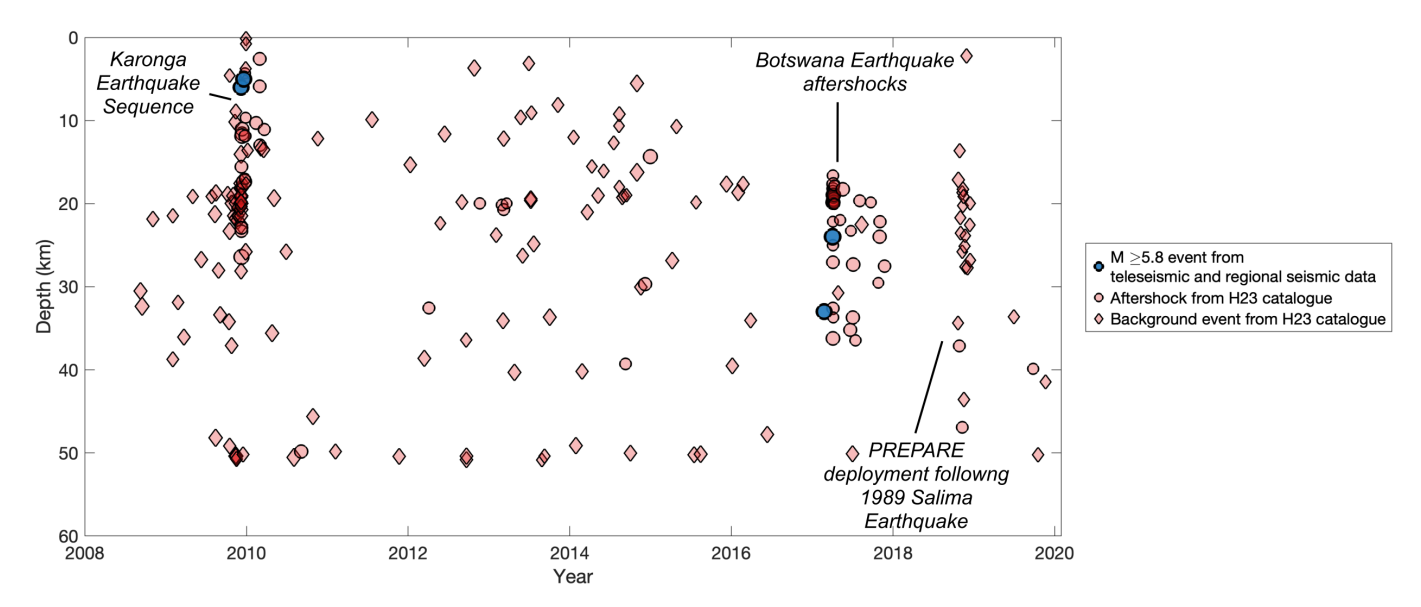


Figure 3 – Temporal and depth correlation between large magnitude earthquakes and events in the H23 relocated catalogue. 'Aftershocks' are events that occurred subsequent to, and within 25 km, of 13  $M_W \geq 5.8$  earthquakes that occurred in the southern EARS between 1980-2020 (*Craig et al.*, 2011; *Craig and Jackson*, 2021). All other H23 events are represented as 'background' events.

## 4 Deep Earthquakes in the Southern East African Rift System; Constraints from Lithospheric Strength Profiles

The causes for deep (>20 km) earthquakes along the southern branches of the EARS have been debated for many years (Buck, 2004; Craig and Jackson, 2021; Fagereng, 2013; Foster and Jackson, 1998; Julià et al., 2005; Nyblade and Langston, 1995; Shudofsky et al., 1987). In addition, it has proved difficult to establish the mechanism responsible for rifting in this region, as the stresses from far-field boundary forces are not sufficient to break the thick, cold lithosphere of southern Africa's metamorphic belts (Kendall and Lithgow-Bertelloni, 2016). In this section, we investigate these questions by developing representative 1-D lithospheric strength profiles for the southern EARS, and then comparing them to the H23 catalogue.

### 4.1 Lithospheric Strength Profiles: Reference Model

Lithospheric strength profiles are developed by evaluating, at depth z, the differential stress required for pressure-dependent frictional deformation or temperature-dependent viscous creep mechanisms (e.g., Brace, 1972;  $Kohlstedt\ et\ al.$ , 1995; Sibson, 1982). The depth over which frictional deformation is favoured in these profiles should therefore coincide with observed earthquake focal depths. Here, we estimate frictional strength using the following equation:

$$(\sigma_1 - \sigma_3) = \alpha \rho z (1 - \lambda_v) \tag{1}$$

where  $(\sigma_1 - \sigma_3)$  is differential stress,  $\alpha$  is a fault parameter (Sibson, 1974),  $\rho$  is density and  $\lambda_v$  is the pore fluid factor (fluid pressure divided by lithostatic

pressure). Here, we set  $\alpha$  to 0.67, which assumes that frictional failure occurs along cohesionless faults that are optimally oriented in an Andersonian normal fault stress regime (i.e.  $\sigma_1$  is vertical) and have a friction coefficient ( $\mu$ ) of 0.6. This assumption is broadly consistent with field observations of cohesionless fault gouges in Malawi (Carpenter et al., 2022; Wedmore et al., 2020b), their favourable orientation for reactivation in Malawi's inferred current stress state (Williams et al., 2019, 2022a) and the frictional strength of felsic rocks sampled from the Malawi Rift (Hellebrekers et al., 2019). Viscous (temperature dependent) strength is estimated by a dislocation creep flow law where:

$$(\sigma_1 - \sigma_3) = \sqrt[n]{\frac{\dot{\varepsilon}}{Ae^{\frac{-Q}{RT}}}} \tag{2}$$

where  $\dot{\varepsilon}$  is the strain rate, A is a material parameter, Q is activation energy, R is the universal gas constant, T is temperature and n is the stress exponent.

In applying Equation 2, T is derived from a 1-D thermal gradient that assumes conductive heat transfer for a crust with a two layer thermal structure:

$$T(z) = T_0 + \frac{Q_0 z}{K_c} - \frac{H_c Z^2}{2K_c}, \quad for \quad z \leq z_{Moho} \quad \ (3)$$

where  $T_0$  and  $Q_0$  are the temperature and heat-flow at the top of each thermal layer,  $K_c$  is crustal thermal conductivity, and  $H_c$  is volumetric heat production (Chapman, 1986; Ranalli, 1995). Following Fagereng (2013),  $K_c$  and  $H_c$  in the upper crust ( $z \leq z_1$ , where  $z_1$  is 9 km) are set to:  $K_{uc}=2.8~Wm^{-1}K^{-1}$  and  $H_{uc}=2.1~\mu Wm^{-3}$ ; and  $K_{lc}=2.0~Wm^{-1}K^{-1}$ ;  $H_{lc}=0.4~\mu Wm^{-3}$  in the lower crust ( $z_1 < z \leq z_{Moho}$ ). For the

lithospheric mantle, we follow the approach of *Afonso* and *Ranalli* (2004) where:

$$\begin{split} T(z) &= -\frac{H_{m}z^{2}}{2K_{m}} + \\ &z \left[ z_{Moho} \left( \frac{H_{m}}{K_{m}} - \frac{H_{lc}}{K_{lc}} \right) + \frac{z_{1}H_{lc}}{K_{lc}} \right] + \\ &z \left[ \frac{Q_{m}}{K_{uc}} + \frac{H_{lc}(z_{Moho} - z_{1})}{K_{uc}} \right] + \\ &T(z_{Moho}) + z_{Moho}^{2} \left( \frac{H_{lc}}{K_{lc}} - \frac{H_{m}}{2K_{m}} \right) - \\ &z_{Moho} \left[ \frac{z_{1}H_{lc}}{K_{lc}} + \frac{Q_{m}}{K_{uc}} + \frac{H_{lc}(z_{Moho} - z_{1})}{K_{uc}} \right], \\ &for \quad z > z_{Moho} \end{split}$$

Here,  $K_m$  and  $H_m$  are the mantle thermal conductivity and volumetric heat production and are set to 0.006  $\mu W m^{-3}$  and 3.0  $W m^{-1} K^{-1}$  respectively (Afonso and Ranalli, 2004).  $Q_m$  is the mantle heat flow across the Moho, and is derived from the difference between surface heat flow and the crust's total heat production,  $\sum_{i=1}^{i=n} H_i zi$ , where  $H_i$  and  $z_i$  represents the heat production and thickness of layer i. The depth to the Moho  $(z_{Moho})$  is set to 41 km, which is the median value of receiver function estimates of Moho depth in this region (Figure 2).

To explore the lithospheric strength profiles' sensitivity to different rheologic parameterisations, we generate a set of profiles that explore variations in: (1) pore fluid pressure, (2) a hydrous lower crust, (3) strain rate, (4) lower crust composition, and (5) surface heat flow. In our initial set of profiles, and consistent with global measurements of crustal stress magnitudes (Townend and Zoback, 2000), we assume hydrostatic pore fluid pressure ( $\lambda_v = 0.4$ ), although there may be some parts of the EARS where pore fluid pressure is lower than hydrostatic (Fagereng et al., 2024).

Surface heat flow values  $(Q_s$ , defines  $Q_0$  for the top crustal layer in Equation 3) vary significantly across southern Africa (e.g., Nyblade et al., 1990). As we are interested in understanding the depth of earthquakes that predominately occur within the rifted lithosphere, we extracted surface heat flow measurements from the Global Heat Flow Database that are within 75 km of a rift branch (Figure 4; Fuchs et al., 2021a,b). exclude early measurements from Lake Malawi and Lake Tanganyika that indicated heat flows  $< 25 \text{ } mWm^{-2}$ (Degens et al., 1971; Von Herzen and Vacquier, 1967) as these have since been corrected for sediment compaction effects or reflect measurements made in disturbed sediments (Ebinger, 1989; Ebinger et al., 1987). Our compilation indicates heat-flow measurements within the western and southwestern rift branches are generally between  $45-80~mWm^{-2}$  (Figure 4) with a mean  $Q_s$  of  $65 \ mWm^{-2}$ . These estimates are consistent with maps of surface heat-flow in the Malawi Rift that are inferred from the Curie point depth ( $\sim 60-75~mWm^{-2}$ ; Njinju et al., 2019b). In our reference lithospheric strength

profiles, we adopt a thermal structure for the crust using the mean estimate for  $Q_s$  (65  $mWm^{-2}$ ) along with a  $T_s=15^{\circ}C$ . Initially, strain rate is set to  $3\cdot 10^{-16}s^{-1}$ , which is approximately equivalent to an extension rate of 1  $mm\ yr^{-1}$  distributed evenly across a 100 km wide rift (Wedmore et al., 2021). The viscous strength of the upper and lower crust are estimated using the flow laws for dry quartz (Rutter and Brodie, 2004) and anorthite (Rybacki and Dresen, 2000) respectively (Tables 2 and 3).

Using the initial conditions outlined above, the frictional-viscous transition (FVT) depth is 32 km (Figure 5b, Table 3). Hence our initial model indicates a FVT depth that is greater than normal continental crust, but shallower than the  $d_{95}$  estimates for the southern EARS (Table 1 and Figure 2). The temperature at the FVT is approximately 700 °C, consistent with suggestions by Mckenzie et al. (2005) for a thermally-dependent seismogenic zone in both oceanic and continental crust. The heat flow value used, combined with the 41 km thick crust, means that the mantle lithosphere is essentially thermally insulated from relatively high stresses in the frictional crust by the lower-stress viscous flow immediately above the Moho. By contrast, for a representative strength profile in Malawi with a felsic lower crust, Fagereng (2013) estimated a FVT depth of 18-20 km. The deeper FVT we estimate reflects the lower strain rate (3  $\cdot$  $10^{-16}~s^{-1}~vs.~10^{-15}~s^{-1}$ ) and differences in flow laws used to approximate the strength of the lower crust (Fagereng (2013) adopted the flow law of Wilks and Carter (1990) for dry quartzofeldspathic granulite).

#### 4.2 Role of Fluids

The presence of fluids has been proposed enable lower-crustal earthquakes Magadi-Natron-Manyara basins of Tanzania Kenya (Roecker et al., 2017), Ethiopian Rift (Muluneh et al., 2021), the Tanganyika Rift (Kolawole and Ajala, 2024; Lavayssière et al., 2019), and the 2017  $M_W$  6.5 Botswana Earthquake (Gardonio et al., 2018; Paulssen et al., 2022). Sun et al. (2021) also suggest that  $V_P/V_S$  ratios 1.8-1.86 in southern Malawi reflect deep "fluid-filled" faults; however, we highlight that this interpretation of elevated  $V_P/V_S$  values does not necessarily imply suprahydrostatic pore fluid pressures (Nishimura et al., 2019).

Here, we examine how fluids might embrittle the lower crust by progressively increasing  $\lambda_v$  from hydrostatic -as in our reference model- to near lithostatic ( $\lambda_v = 0.9$ ). In the extreme case with  $\lambda_v = 0.9$ , the FVT is suppressed to 35 km (Figure 6a). Hence, in the context of these strength profiles, increasing  $\lambda_v$  does increase the depth to the FVT, but cannot account for the seismicity occurring at 35-40 km depths in the southern EARS (Figure 2, Table 1). In addition, a 'hydrous' lower crust implies that dislocation creep is more appropriately modelled using flow laws for wet lithologies (Afonso and Ranalli, 2004; Tulley et al., 2020). Substituting flow laws for wet quartz (Kirby and Kronenberg, 1987), anorthosite

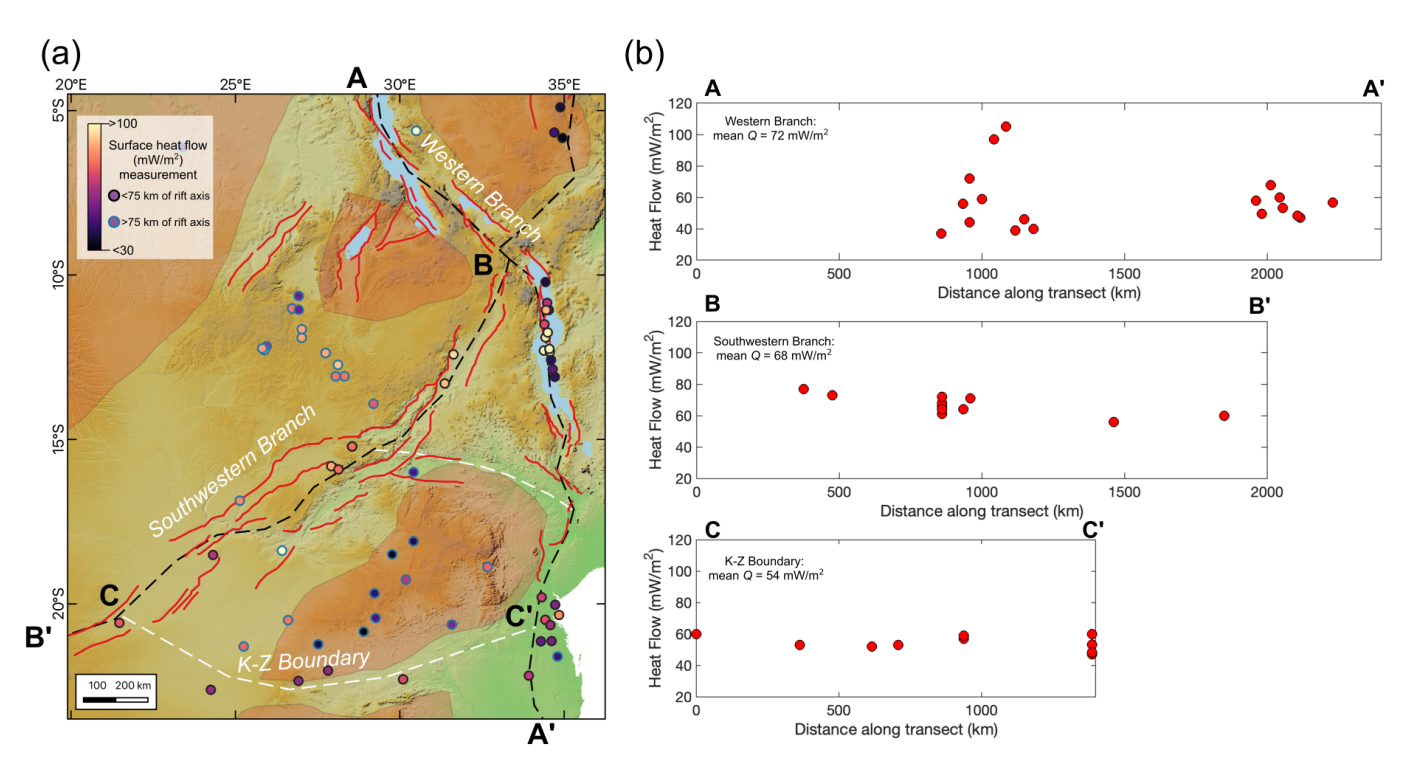


Figure 4 – (a) Heat-flow compilation from across southeastern Africa from the Global Heat Flow Database (Fuchs et al., 2021a,b). Faults (red lines) and rift axes (black and white dashed lines) as in Figure 1. (b) Along-rift transects that select heat-flow measurements < 75 km from the rift branch axes.

Table 2 – Parameters used in the application of Equations 1 and 2 for the 1-D lithospheric strength profiles.

| Lithology     | $(MPa^{-n} \cdot s^{-1})$ | n   | $E \ (kJ \cdot mol^{-1})$ | $(kg \cdot m^{-3})$ | Reference                   |
|---------------|---------------------------|-----|---------------------------|---------------------|-----------------------------|
| Quartzite-dry | $1.3 \cdot 10^{-5}$       | 3   | 242                       | 2650                | Rutter and Brodie (2004)    |
| Quartzite-wet | $3.2 \cdot 10^{-4}$       | 2.3 | 154                       | 2650                | Kirby and Kronenberg (1987) |
| Anorthite-dry | $5.0 \cdot 10^{12}$       | 3   | 648                       | 2800                | Rybacki and Dresen (2000)   |
| Anorthite-wet | 398                       | 3   | 356                       | 2800                | Rybacki and Dresen (2000)   |
| Diabase dry   | 8.0                       | 4.7 | 485                       | 2900                | Mackwell et al. (1998)      |
| Olivine-dry   | $1.1 \cdot 10^{5}$        | 3.5 | 530                       | 3320                | Hirth and Kohlstedt (2003)  |
| Olivine-wet   | 1600                      | 3.5 | 520                       | 3320                | Hirth and Kohlstedt (2003)  |

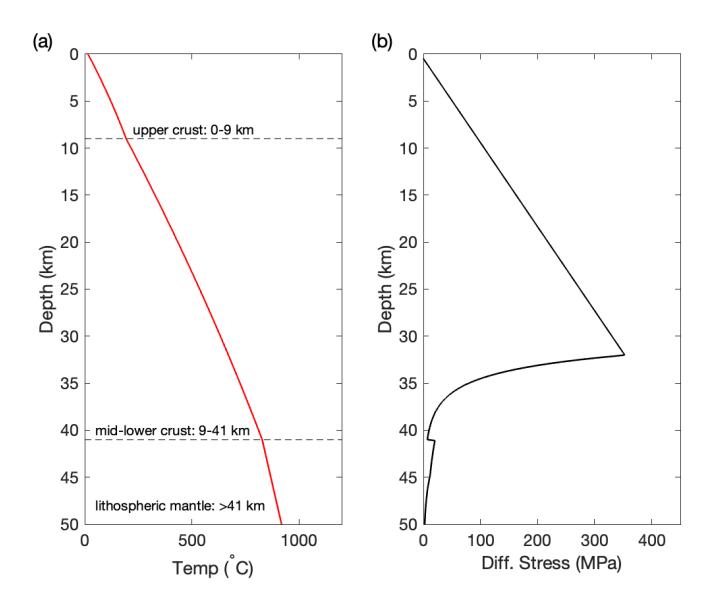


Figure 5 – (a) Geotherm and (b) lithospheric strength for the initial set of conditions when parameterising Equations 1-3.

(Rybacki and Dresen, 2000), and olivine (Hirth and Kohlstedt, 2003) into Equation 2 (Table 2), the FVT is modelled to extend to only 21-25 km (Figure 6b, Table 3). Accounting for seismicity in a hydrous lower crust is also challenging as: (1) this would promote retrograde growth of fine-grained phyllosilicate minerals, which at lower crustal conditions are more susceptible to viscous or aseismic creep mechanisms (Craig and Jackson, 2021; Fagereng et al., 2024; Wintsch et al., 1995), and (2) a hydrous crust would also have a lower melting point (Fagereng et al., 2024) potentially allowing partial melting and associated weakening of the crust (Rosenberg and Handy, 2005).

#### Lateral Heterogeneities in the 4.3 Lower Crust

We next investigate if frictional failure in the lower crust is driven by deformation localising along smaller-scale structures within the rift, and which in turn, implies that strain rates around these structures are higher than if strain was equally partitioned across the southern EARS (Birhanu et al., 2016; Wedmore et al., 2021).

Table 3 – Summary of the model constraints for the lithospheric strength profiles in figures 5 and 6, and their predictions for properties of the frictional viscous transition zone in the southern EARS.

| Model | Crustal composition  | $\begin{array}{c} \textbf{Pore fluid} \\ \textbf{factor} \\ \lambda_v \end{array}$ | $\begin{array}{c} \textbf{Strain rate} \\ \dot{\varepsilon}(s^{-1}) \end{array}$ | Surface  | Frictional-viscous transition properties |   |                              |
|-------|--|--|--|--|--|---|------------------------------|
|       |  |  |  | $\begin{array}{c} \textbf{heat flow} \\ Q_s(mWm^{-2}) \end{array}$ | Depth (km)                               | $\begin{array}{c} \text{Temperature} \\ (^{\circ}\text{C}) \end{array}$ | Differential<br>stress (MPa) |
| 1     | 0-9 km: dry quartz<br>9-41 km: dry feldspar                    | 0.4  | $3 \cdot 10^{-16}$   | 65   | 32                                       | 670   | 355                          |
| 2a-e  | 0-9 km: dry quartz<br>9-41 km: dry feldspar                    | 0.4-0.9  | $3\cdot 10^{-16}$  | 65   | 32-35                                    | 670-730   | 65-355                       |
| За-е  | 0-9 km: wet quartz<br>9-41 km: wet feldspar                    | 0.4-0.9  | $3\cdot 10^{-16}$  | 65   | 21-25                                    | 465-530   | 45-235                       |
| 4а-е  | 0-9 km: dry quartz<br>9-41 km: dry feldspar                    | 0.4  | $3\cdot 10^{-16} - 3\cdot 10^{-11}$  | 65   | 32-40                                    | 670-815   | 350-440                      |
| 5     | 0-9 km: dry quartz<br>9-30 km: dry feldspar<br>30-41 km: mafic | 0.4  | $3\cdot 10^{-16}$  | 65   | 32                                       | 670   | 355                          |
| 6а-с  | 0-9 km: dry quartz<br>9-41 km: dry feldspar                    | 0.4  | $3\cdot 10^{-16}$  | 45-80  | 24-99                                    | 610-680   | 225-1220                     |

Considering scenarios where 1  $mm~yr^{-1}$  of extension is accommodated across zones from 100 km to 1 m wide, the resulting strain rate changes from  $\sim 3 \cdot 10^{-16}$  to  $\sim 3 \cdot 10^{-11}~s^{-1}$ . This has the effect of increasing the depth at which brittle failure is possible from 32 km to  $\sim 40$  km (Figure 6c).

#### 4.4 Mafic Lower Crust

Crustal strength profiles have previously been used to suggest that a dry mafic lower crust can account for a 30-35 km deep FVT in southern Africa (Albaric et al., 2014; Fagereng, 2013; Nyblade and Langston, 1995; Shudofsky et al., 1987). This reflects that at comparable temperatures, the viscous strength of dry mafic rocks is typically greater than quartzofeldspathic rocks (Mackwell et al., 1998), and a mafic composition has been proposed to embrittle the lower crust in other regions (Déverchère et al., 2001; Williams et al., 2025). Mafic granulites are also more prone to unstable frictional sliding, as opposed to stable, aseismic creep, at lower crustal temperatures (Hellebrekers et al., 2019).

Locally elevated bulk crustal  $V_P/V_S$  ratios (>1.8) beneath the southern end of Lake Tanganyika suggest the presence of mafic granulites at lower crustal pressures ( $V_P/V_S$  of mafic granulite at 600 GPa is 1.82, Figure 2a; Christensen, 1996; Hodgson et al., 2017). Furthermore, most Precambrian terranes (including both cratonic and Proterozoic crust) in southern Africa have elevated shear wave velocities (4.0-4.3 km s<sup>-1</sup>) in the lower crust implying a mafic layer with an average thickness of 6  $\pm$  3 km (Julià et al., 2005; Kachingwe et al., 2015).

We note, however, that the elevated  $V_P/V_S$  ratios beneath Lake Tanyanyika may instead represent lower crustal melts (Ajala et al., 2024). Furthermore,  $V_P/V_S$  ratios indicate a mafic layer is absent beneath the Bangweulu Block (Kachingwe et al., 2015), Luangwa Rift (Sun et al., 2021), and the northern Malawi Rift (Borrego et al., 2018). Indeed, the median bulk crustal  $V_P/V_S$  ratio along the Western Branch of the EARS is 1.74, which is consistent with a felsic-granulite composition for the mid- to lower crust (Borrego et al., 2018; Kachingwe et al., 2015). Moreover, the 1D strength profiles we

developed using a flow law for dry mafic crust (Table 2) indicate that: (1) the lower crust is not necessarily stronger than a profile with a felsic (dry anorthite) flow law, and (2), unless a low geothermal gradient/elevated strain rate is considered, a mafic composition still fails to account for seismicity at depths >30 km (Figure 6d, Table 3).

#### 4.5 Influence of Geothermal Gradient

incorporate uncertainty in southern Africa's geotherm, we show strength profiles with surface heat flow  $(Q_s)$ , -which represents  $Q_0$  for the upper crustal layer in Equation 3- set to 45, 65, and 80  $mW m^{-2}$ (Figure 6e and f). This encapsulates the range of surface heat flow measurements within the southern EARS (Figure 4). In the case  $Q_s = 45 \ mW \ m^{-2}$ , the entire crust and upper lithospheric mantle (depths < 99 km) is predicted to be seismogenic (Figure 6f). This is inconsistent with the  $d_{95}$  estimates from the H23 catalogue (Table 1), and so we do not consider that this end-member lithospheric strength profile is realistic. Nevertheless, it requires only a slightly lower surface heat flow than used in our reference profile  $(56 \text{ } vs. 65 \text{ } mW \text{ } m^{-2})$  for a FVT depth that is consistent with the  $d_{95}$  estimates from the H23 catalogue. A depressed geotherm could therefore account for lower crustal seismicity in southern Africa. However, there are also regions, such as central Malawi and the Okavango Rift, where the surface heat flow is relatively high  $(\sim 70 - 80 \text{ mW m}^{-2})$ , Figure 4; Njinju et al., 2019b; Fuchs et al., 2021b) and lower crustal earthquakes are known to occur (Figure 2). Hence, a low geothermal gradient alone cannot account for widespread lower crustal earthquakes in the southern EARS.

#### 4.6 Transient Localisation of Strain

There is a wealth of evidence that transient deformation occurs following earthquakes (Biggs et al., 2010; Ingleby and Wright, 2017; Lloyd et al., 2019; Wright et al., 2013), as is also evident in the H23 catalogue (Figure 3). Although the exact mechanism of transient postseismic deformation is debated, a uniform observation is that

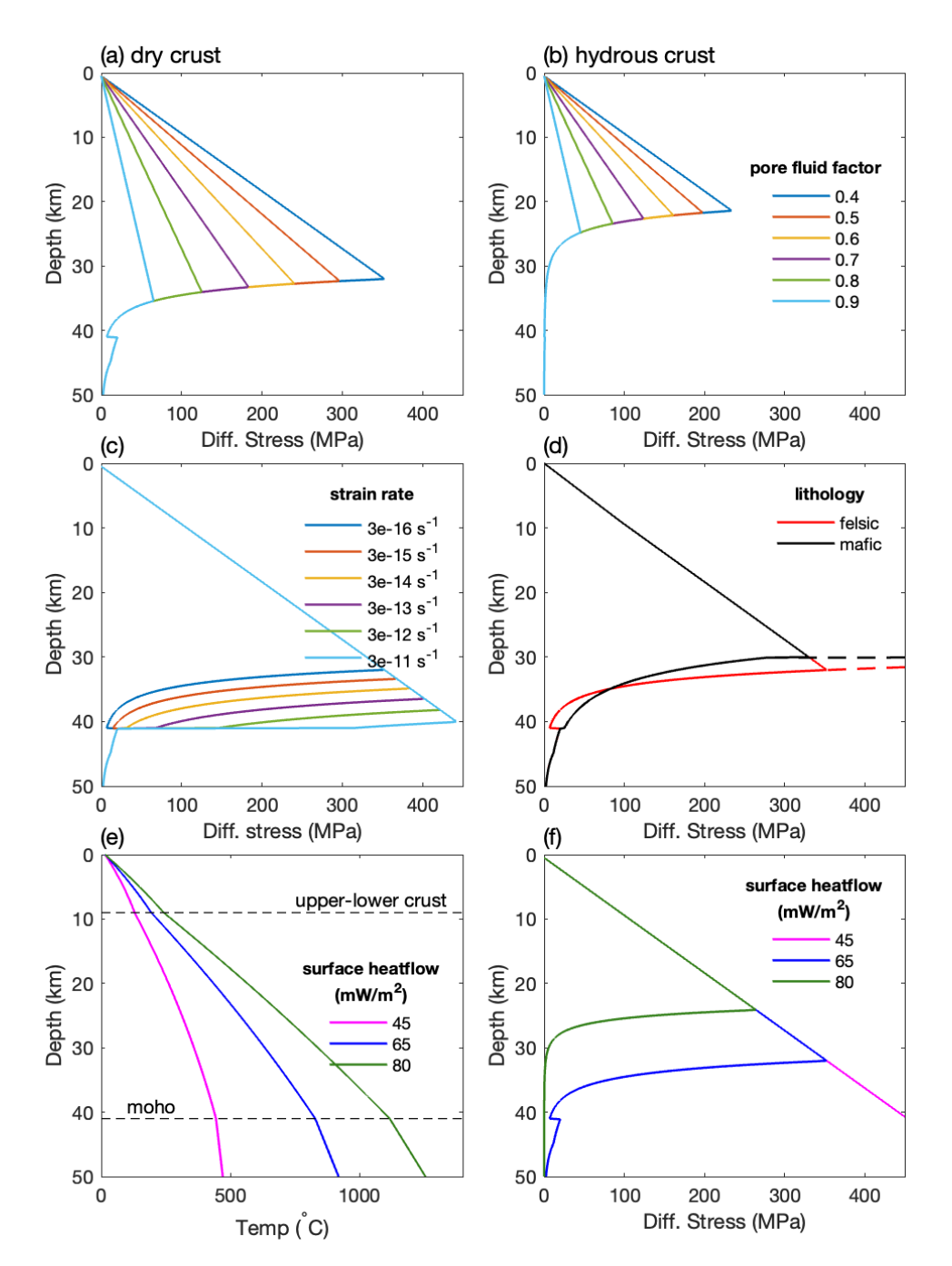


Figure 6 – Representative lithospheric strength profiles for the southern EARS, indicating how the depth to the frictional viscous transition (FVT) varies depending on the parameterisation of Equations 1-3. (a & b) Effects of varying pore fluid pressure between hydrostatic ( $\lambda_v = 0.4$ ) and near lithostatic ( $\lambda_v = 0.9$ ) in Equation 1, and assuming (a) dry and (b) wet viscous strength flow laws (Table 2). (c) The effect of varying the width over which rift extension occurs between 100 km and 1 m, and the consequent changes in strain rate, on the depth to the FVT. (d) Comparison of strength profiles for a felsic lower crust (equivalent to Figure 5b) and where the lower crust is comprised of a mafic layer between 30-41 km depth. (e) Geothermal gradient and (f) lithospheric strength profiles that encapsulate a range of surface heat flow measurements for the southern EARS (Figure 4). A summary of how these profiles have been parameterised, and their influence on the FVT, is collated in Table 3.

postseismic velocity is inversely proportional to the time since the earthquake, and modelling of these velocity measurements suggests that most deformation is the result of fault zone processes (Ingleby and Wright, 2017). To consider the change in strain rate following an earthquake we use a power law shear zone model (Montési, 2004), where the postseismic surface velocity,  $V_s$ , changes with time t as:

$$V_s(t) = V_0 \left[ 1 + \left( 1 - \frac{1}{n} \right) \frac{1}{\tau} \right]^{\frac{-1}{(1 - \frac{1}{n})}} \tag{5}$$

where  $V_0$  and  $\tau$  are constants describing the instantaneous postseismic velocity, and the relaxation time respectively, and n is a power law exponent. Although this relaxation law models the surface velocity, by considering that shear zone velocity is proportional to surface velocity and varying the width of the shear zones

in which this postseismic deformation is accommodated (shear zones 1 m, 10 m and 100 m wide), we calculate the strain rate and how this varies with time following an earthquake (Figure 7). We then use the values of strain rate to calculate the viscous stress (Equation 2) at different times since an earthquake. values of 500 mm/yr and 0.09 yrs for  $V_0$  and  $\tau$ , as these provide a plausible fit to post-seismic velocities recorded following the 2006  $M_W$  7.0 Machaze Earthquake (Copley et al., 2012). Using these values, the strain rate rapidly decreases following the first year of post-seismic deformation, regardless of the power law exponent or shear zone width. Overall, it takes over 1,000 years for postseismic strain rates to reduce below background levels of  $1 \cdot 10^{-16} \ s^{-1}$ , unless n tends to 1 (Figure 7). However, in the case of n = 1, Equation 5 tends to one that matches the linear Maxwell law for postseismic deformation, which has shown to be a poor fit to postseismic velocity measurements (Ingleby and Wright, 2017).

Assuming the postseismic deformation accommodated across a single 10 m wide shear zone, the increase in strain rate in the immediate post-seismic period (< 1 year) results in an increase in the FVT down to the Moho (Figure 7). As the strain rates decreases in the tens to hundreds of years following the earthquake, the depth of the FVT decreases, but it remains deeper than that of the background strain rate for >1,000 years (Figure 7). Hence, a simple model of post-seismic deformation in shear zones increases the depth to the FVT following large magnitude earthquakes, and in turn allows frictional failure down to the Moho. This transient embrittlement of the lower crust is consistent with the observation from the H23 catalogue, in which mainshocks are often shallower than their subsequent aftershocks (Figure 3), and with studies elsewhere (Ben-Zion and Lyakhovsky, 2006; Rolandone et al., 2004). In addition to elevated strain rates, lower crustal aftershocks may also be driven by the stress increases, fracturing, and fluid flow from upper crustal earthquakes (Jamtveit et al., 2018). We also note that this mechanism cannot account for lower crustal mainshocks within the southern EARS, such as the 1989  $M_W$ 6.1 Salima Earthquake and 2017  $M_W$ 6.5 Botswana Earthquake (focal depths  $32 \pm 5$  km and 29 $\pm$  4 km respectively).

#### 5 Discussion

There are a number of mechanisms that can embrittle the lower crust in southeastern Africa. For example, our 1-D lithospheric strength profiles are consistent with previous studies that suggest a low geothermal gradient and/or mafic lower crust are viable mechanisms for driving lower crustal seismicity (Albaric et al., 2014; Fagereng, 2013; Nyblade and Langston, 1995; Shudofsky et al., 1987). Crucially, however, the H23 catalogue indicates that there are sections of the southern EARS, such as the Malawi and Luangwa rifts, where deep seismicity occurs within a felsic lower crust with a relatively elevated geothermal gradient (i.e., surface heat flow >60

 $mW m^{-2}$ ).

The migration of crustal and mantle fluids can also trigger lower crustal seismicity in the southern branches of the EARS, typically in the form of M < 4 earthquake swarms (Kolawole and Ajala, 2024; Lavayssière et al., 2019; Lindenfeld et al., 2012b). There are, however, also regions where fluid-driven mechanisms for lower crustal seismicity are less obvious. For example, the 32 km deep  $M_W$  6.1 Salima Earthquake in southern Malawi nucleated in a region where: (1) metamorphic reactions have dehydrated the lower crust (Fagereng et al., 2024; Manda et al., 2019), (2) possible incursion of meteoric fluids from above can be excluded as hot springs in this region indicate that they percolate to depths < 5 km (Dávalos-Elizondo et al., 2021), and (3) there is no evidence from  $V_P/V_S$  measurements for upper mantle upwelling or partial melting (Sun et al., 2021). Moreover, our 1-D strength profiles indicate that elevated pore fluid pressures are not an effective mechanism for increasing the FVT depth in the southern EARS (Figure 6a), particularly if sufficient water is present that it ultimately promotes viscous or aseismic (Figure 6b; Craig and Jackson, 2021; Fagereng et al., 2024; Wintsch et al., 1995). We highlight too that these 1-D strength profiles do not consider the possibility that near-lithostatic fluid pressures are difficult to maintain in a normal fault stress state (Sibson, 2000; Sibson and Rowland, 2003), or alternatively, that elevated pore fluid pressures are 'ineffective' at reducing effective stresses in the lower crust (Hirth and Beeler, 2015).

We therefore propose that an additional mechanism for driving lower crustal seismicity in the southern EARS are across-rift regions with elevated strain rates. In Figure 6c, we show how decreasing the width of the zone of deformation from 100 km to 1 m, and thus increasing the strain rate, can increase the depth of the frictional-viscous transition to depths approaching the Moho. This degree of across-rift strain localisation is consistent with the observation that, given their length and displacement, southern EAR fault zones are relatively narrow as they have inherited underlying viscous shear zones (Carpenter et al., 2022; Hodge et al., 2018; Wedmore et al., 2020b; Williams et al., 2022b). In particular, relatively strong blocks that surround viscously deforming strands within these shear zones may be favourable sites for lower crustal earthquake nucleation (Campbell et al., 2020; Zertani et al., 2025). This is consistent with the hypothesis that weak viscous shear zones that localise strain are a requirement to allow rifting of the otherwise strong African lithosphere (Fagereng et al., 2024; Kendall and Lithgow-Bertelloni, 2016). We also note that high strain rates may actually be a prerequisite for earthquakes to nucleate within a predominantly felsic lower crust, as these rocks tend to be velocity-strengthening but become more unstable with higher strain rate (Hellebrekers et al., 2019).

We also demonstrate how transient post-seismic deformation increase strain rates, which in turn, can also facilitate earthquakes at greater depths (Figure 7). This localisation occurs in both space, within shear zones

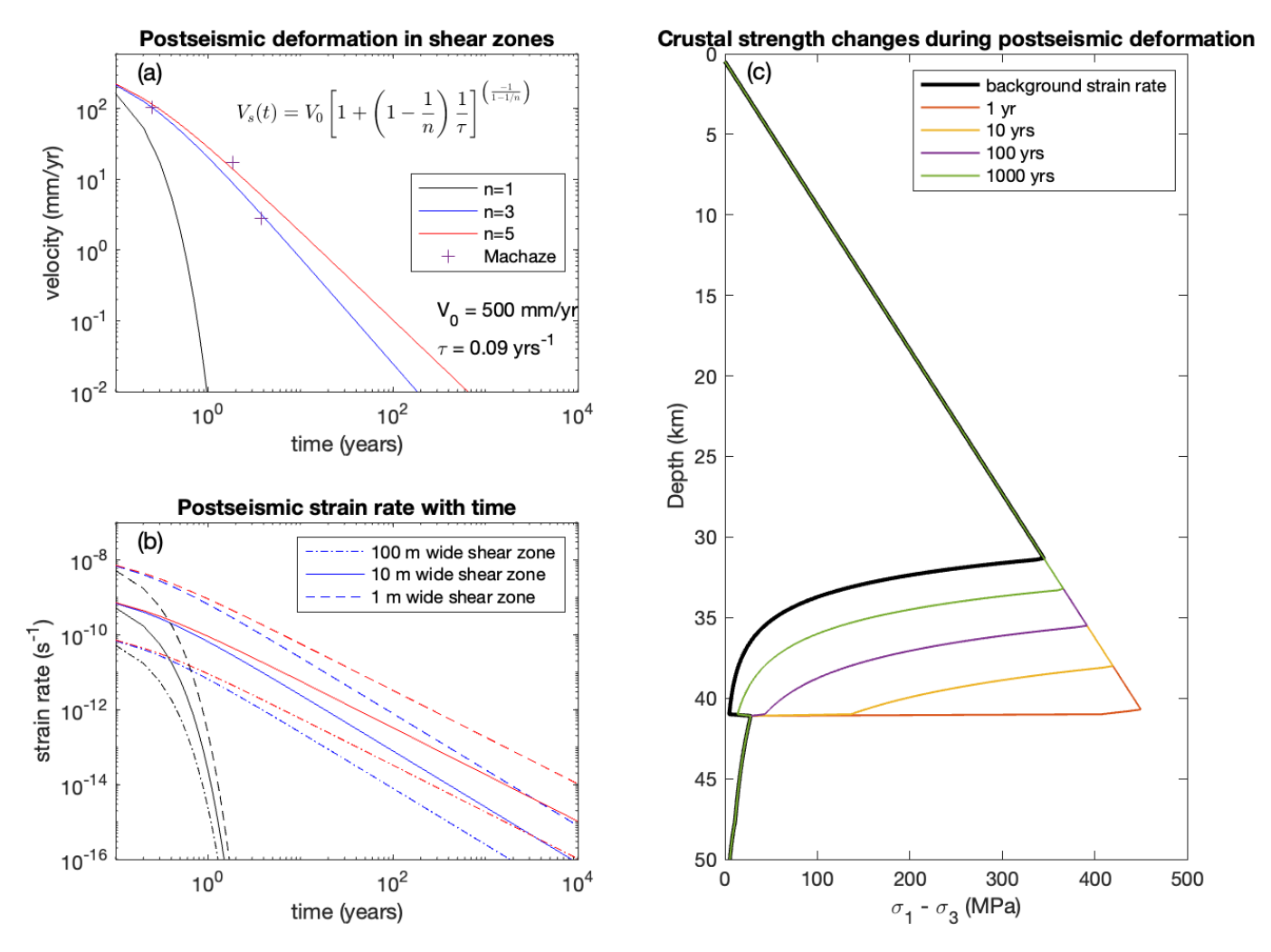


Figure 7 – Strain localisation following large earthquakes. a) postseismic velocities at the surface for power law exponents (n) of 1,3 and 5. The crosses show post-seismic velocities following the 2006  $M_W$  7.0 Machaze Earthquake in Mozambique (Copleyet al., 2012; Ingleby and Wright, 2017). b) Change in postseismic strain rates with time within a shear zone of widths 1, 10 and 100 m and different values of n (line colours as in panel a), and c) effect on lithospheric strength with time after major earthquake for a 10 m wide shear zone and power law exponent of n = 3.

below seismogenic faults, and in time, as the increased strain rate decays with time since the earthquake (Figure 7). Long (>80 km) active faults and multimetre single event displacements, imply that M >7 earthquakes are possible along the length of the western and southwestern branches (Grant et al., 2024; Hodge et al., 2020; Jackson and Blenkinsop, 1997; Kinabo et al., 2008; Wedmore et al., 2022; Williams et al., 2022c). Thus, transient post-seismic deformation may enhance the seismogenic thickness around past earthquake ruptures within these EARS branches. Our modelling suggests that postseismic deformation following the 2006  $M_W$  7.0 Machaze Earthquake provides a good fit to a model where deformation is driven by slip within shear zones with a power law exponent > 1 (Ingleby and Wright, 2017; Montési, 2004). Given the constraints in the model, and the low overall strain rates in East Africa, if regional lower crustal seismicity is driven by post-seismic deformation after larger earthquakes, then strain rates and the depth to the FVT will remain elevated above background levels for hundreds to thousands of years.

#### Conclusions 6

We use the new catalogue of relocated earthquakes in southeastern Africa compiled by Holmgren et al. (2023) to investigate the mechanisms driving deep earthquakes in this region. Unlike previous studies which used teleseismic catalogues, this catalogue is based on temporary seismic deployments that have taken place over the last 20 years and thus is heterogeneously distributed in space and time. From this catalogue we derive  $d_{95}$  estimates -the depth above which 95% of seismicity occurs- of 50 and 36 km for the Western Branch and between the Kapvaal and Zimbabwe cratons. A mafic lower crust, low geothermal gradient, and the presence of fluids may locally contribute to this observation. However, in some rift segments, the lower crust is neither mafic, wet, nor particularly cold. In these regions, and possibly elsewhere along the southern EARS, we propose that spatial-temporal elevations in strain rate are a key factor driving lower crustal earthquakes.

## Acknowledgements

This work was funded by a number of EPSRC grants funded under the Global Challenges Research Fund (GCRF): PREPARE (EP/P028233/1); SAFER PREPARED (part of the "Innovative data services for aquaculture, seismic resilience, and drought adaptation in East Africa" grant; EP/T015462/1); a GCRF EPSRC Institutional Sponsorship Award and an EPSRC Impact Accelerator Award (grant no. EP/R511663/1). We thank the editors and three reviewers for their helpful comments.

### Author contributions

Conceptualization: all authors Data curation: LW, JW, and JH Formal analysis: LW and JW

Funding acquisition: JB, MW, and AF

Writing - original draft: LW

Writing - reviewing and editing: all authors

## Data availability

A compilation of the Moho depth estimates and  $V_P/V_S$  measurements in southern Africa is included as a Supplementary File. The Holmgren et al. (2023) catalogue is available at https://doi.org/10.31905/4GGVBFBE, and the surface heat-flow measurements compiled by Fuchs et al. (2021b) and shown in Figure 4 are available at https://doi.org/10.5880/fidgeo.2021.014.

## Competing interests

The authors declare no competing interests.

#### Peer review

This publication was peer-reviewed by Ameha Muluneh, Folarin Kolawole, and Rasheed Ajala. The full peer-review report can be found here: Review Report.

## Copyright notice

© Author(s) 2025. This article is distributed under the Creative Commons Attribution 4.0 International License, which permits unrestricted use, distribution, and reproduction in any medium, provided the original author(s) and source are credited, and any changes made are indicated.

#### References

- Afonso, J. C., and G. Ranalli (2004), Crustal and mantle strengths in continental lithosphere: is the jelly sandwich model obsolete?, *Tectonophysics*, 394(3-4), 221–232, doi: 10.1016/j.tecto.2004.08.006.
- Ajala, R., F. Kolawole, and W. Menke (2024), Blind magmatism abets nonvolcanic continental rifting, Communications earth & environment, 5(1), 1–8, doi: 10.1038/s43247-024-01244-7.

- Albaric, J., J. Déverchère, J. Perrot, A. Jakovlev, and A. Deschamps (2014), Deep crustal earthquakes in North Tanzania, East Africa: Interplay between tectonic and magmatic processes in an incipient rift, Geochemistry, geophysics, geosystems: G(3), 15(2), 374-394, doi: 10.1002/2013gc005027.
- Ambraseys, N. N., and R. D. Adams (1992), Reappraisal of major African earthquakes, south of  $20^{\circ}$ N, 1900-1930, Tectonophysics, 209(1-4), 293-296, doi: 10.1016/0040-1951(92)90036-6.
- Ben-Zion, Y., and V. Lyakhovsky (2006), Analysis of aftershocks in a lithospheric model with seismogenic zone governed by damage rheology, *Geophysical journal international*, 165(1), 197–210, doi: 10.1111/j.1365-246x.2006.02878.x.
- Biggs, J., E. Nissen, T. Craig, J. Jackson, and D. P. Robinson (2010), Breaking up the hanging wall of a rift-border fault: The 2009 Karonga earthquakes, Malawi: THE 2009 KARONGA EARTHQUAKES, MALAWI, Geophysical research letters, 37(11), doi: 10.1029/2010gl043179.
- Biggs, J., A. Ayele, T. P. Fischer, K. Fontijn, W. Hutchison, E. Kazimoto, K. Whaler, and T. J. Wright (2021), Volcanic activity and hazard in the East African Rift Zone, *Nature communications*, 12(1), 6881, doi: 10.1038/s41467-021-27166-y.
- Birhanu, Y., R. Bendick, S. Fisseha, E. Lewi, M. Floyd, R. King, and R. Reilinger (2016), GPS constraints on broad scale extension in the Ethiopian Highlands and Main Ethiopian Rift, *Geophysical research letters*, 43(13), 6844–6851, doi: 10.1002/2016gl069890.
- Borrego, D., A. A. Nyblade, N. J. Accardo, J. B. Gaherty, C. J. Ebinger, D. J. Shillington, P. R. N. Chindandali, G. Mbogoni, R. W. Ferdinand, G. Mulibo, J. P. O'Donnell, M. Kachingwe, and G. Tepp (2018), Crustal structure surrounding the northern Malawi rift and beneath the Rungwe Volcanic Province, East Africa, Geophysical journal international, 215(2), 1410–1426, doi: 10.1093/gji/ggy331.
- Brace, W. F. (1972), Laboratory studies of stick-slip and their application to earthquakes, Tectonophysics, 14(3-4), 189-200, doi: 10.1016/0040-1951(72)90068-6.
- Buck, W. R. (2004), Consequences of asthenospheric variability on continental rifting, in *Rheology and Deformation of the Lithosphere at Continental Margins*, edited by G. D. Karner, B. Taylor, N. W. Driscoll, and D. L. Kohlstedt, pp. 1–30, Columbia University Press, New York Chichester, West Sussex, doi: 10.7312/karn12738-002.
- Campbell, L. R., L. Menegon, A. Fagereng, and G. Pennacchioni (2020), Earthquake nucleation in the lower crust by local stress amplification, *Nature communications*, 11(1), 1322, doi: 10.1038/s41467-020-15150-x.
- Carpenter, M., J. N. Williams, A. Fagereng, L. N. J. Wedmore, J. Biggs, F. Mphepo, H. Mdala, Z. Dulanya, and B. Manda (2022), Comparing intrarift and border fault structure in the Malawi Rift: Implications for normal fault growth, *Journal of structural geology*, 165(104761), 104,761, doi: 10.1016/j.jsg.2022.104761.
- Christensen, N. I. (1996), Poisson's ratio and crustal seismology, *Journal of geophysical research. Solid earth*, 101(2), 3139–3156, doi: 10.1029/95JB03446.
- Copley, A., J. Hollingsworth, and E. Bergman (2012), Constraints on fault and lithosphere rheology from the

- coseismic slip and postseismic afterslip of the 2006  $M_w$ 7.0 Mozambique earthquake: MOZAMBIQUE EARTHQUAKE AND AFTERSLIP, Journal of geophysical research, 117(B3), doi: 10.1029/2011jb008580.
- Craig, T. J., and J. A. Jackson (2021), Variations in the seismogenic thickness of east Africa, *Journal of geophysical research*. *Solid earth*, 126(3), 1–15, doi: 10.1029/2020jb020754.
- Craig, T. J., J. A. Jackson, K. Priestley, and D. Mckenzie (2011), Earthquake distribution patterns in Africa: Their relationship to variations in lithospheric and geological structure, and their rheological implications, Geophysical journal international, 185(1), 403–434, doi: 10.1111/j.1365-246X.2011.04950.x.
- Daly, M. C., P. Green, A. B. Watts, O. Davies, F. Chibesakunda, and R. Walker (2020), Tectonics and landscape of the central African plateau and their implications for a propagating southwestern rift in Africa, Geochemistry, geophysics, geosystems: G(3), 21(6), doi: 10.1029/2019gc008746.
- Degens, E. T., R. P. Von Herzen, and H.-K. Wong (1971), Lake tanganyika: Water chemistry, sediments, geological structure, *The Science of Nature*, 58(5), 229–241, doi: 10.1007/bf00602986.
- Delvaux, D., J.-L. Mulumba, M. N. S. Sebagenzi, S. F. Bondo, F. Kervyn, and H.-B. Havenith (2017), Seismic hazard assessment of the Kivu rift segment based on a new seismotectonic zonation model (western branch, East African Rift system), Journal of African earth sciences (Oxford, England: 1994), 134, 831–855, doi: 10.1016/j.jafrearsci.2016.10.004.
- Dávalos-Elizondo, E., E. A. Atekwana, E. A. Atekwana, G. Tsokonombwe, and D. A. Laó-Dávila (2021), Medium to low enthalpy geothermal reservoirs estimated from geothermometry and mixing models of hot springs along the Malawi Rift Zone, *Geothermics*, 89(101963), 101,963, doi: 10.1016/j.geothermics.2020.101963.
- Déverchère, J., C. Petit, N. Gileva, N. Radziminovitch, V. Melnikova, and V. San'Kov (2001), Depth distribution of earthquakes in the Baikal rift system and its implications for the rheology of the lithosphere, Geophysical journal international, 146(3), 714–730, doi: 10.1046/j.0956-540x.2001.1484.484.x.
- Ebinger, C. J. (1989), Tectonic development of the western branch of the East African rift system, *Geological Society of America bulletin*, 101(7), 885–903, doi: 10.1130/0016-7606(1989)101<0885:TDOTWB>2.3.CO;2.
- Ebinger, C. J., B. R. Rosendahl, and D. J. Reynolds (1987), Tectonic model of the Malaŵi rift, Africa, Tectonophysics, 141(1-3), 215-235, doi: 10.1016/0040-1951(87)90187-9.
- Ebinger, C. J., S. J. Oliva, T.-Q. Pham, K. Peterson, P. Chindandali, F. Illsley-Kemp, C. Drooff, D. J. Shillington, N. J. Accardo, R. J. Gallacher, J. Gaherty, A. A. Nyblade, and G. Mulibo (2019), Kinematics of active deformation in the Malawi rift and Rungwe Volcanic Province, Africa, *Geochemistry, geophysics, geosystems:* G(3), 20(8), 3928-3951, doi: 10.1029/2019gc008354.
- Fagereng, A. (2013), Fault segmentation, deep rift earthquakes and crustal rheology: Insights from the 2009 Karonga sequence and seismicity in the Rukwa–Malawi rift zone, *Tectonophysics*, 601, 216–225, doi: 10.1016/j.tecto.2013.05.012.
- Fagereng, A., J. F. A. Diener, C. J. Tulley, and B. Manda (2024), Metamorphic inheritance,

- lower-crustal earthquakes, and continental rifting, Geochemistry, geophysics, geosystems: G(3), 25(3), doi: 10.1029/2023gc011305.
- Fonseca, J. F. B. D., J. Chamussa, A. Domingues, G. Helffrich, E. Antunes, G. van Aswegen, L. V. Pinto, S. Custodio, and V. J. Manhica (2014), MOZART: A seismological investigation of the east African rift in central Mozambique, Seismological research letters, 85(1), 108–116, doi: 10.1785/0220130082.
- Foster, A. N., and J. A. Jackson (1998), Source parameters of large African earthquakes:implications for crustal rheology and regional kinematics: Source parameters of large African earthquakes, *Geophysical journal international*, 134(2), 422–448, doi: 10.1046/j.1365-246x.1998.00568.x.
- Fuchs, S., G. Beardsmore, P. Chiozzi, O. M. Espinoza-Ojeda,
  G. Gola, W. Gosnold, R. Harris, S. Jennings, S. Liu,
  R. Negrete-Aranda, F. Neumann, B. Norden, J. Poort,
  D. Rajver, L. Ray, M. Richards, J. D. Smith, A. Tanaka,
  and M. Verdoya (2021a), A new database structure for the
  IHFC Global Heat Flow Database, International Journal
  of Terrestrial Heat Flow and Applications, 4(1), 1–14, doi:
  10.31214/ijthfa.v4i1.62.
- Fuchs, S., B. Norden, and International Heat Flow Commission (2021b), The Global Heat Flow Database: Release 2021, doi: 10.5880/FIDGEO.2021.014.
- Gaherty, J. B., W. Zheng, D. J. Shillington, M. E. Pritchard, S. T. Henderson, P. R. N. Chindandali, H. Mdala, A. Shuler, N. Lindsey, S. J. Oliva, S. Nooner, C. A. Scholz, D. Schaff, G. Ekström, and M. Nettles (2019), Faulting processes during early-stage rifting: seismic and geodetic analysis of the 2009–2010 Northern Malawi earthquake sequence, *Geophysical journal international*, 217(3), 1767–1782, doi: 10.1093/gji/ggz119.
- Gardonio, B., R. Jolivet, E. Calais, and H. Leclère (2018), The April 2017  $M_w 6.5$  Botswana earthquake: An intraplate event triggered by deep fluids, *Geophysical research letters*, 45(17), 8886–8896, doi: 10.1029/2018gl078297.
- Gounon, A., J. Letort, F. Cotton, G. Weatherill, M. Sylvander, and S. Latour (2021), Improving depth estimations of African earthquakes using teleseismic data, and influence for the East-African rift seismic hazard characterization, *Geophysical journal international*, 228(1), 447–460, doi: 10.1093/gji/ggab348.
- Grant, C., F. Kolawole, and J. Williams (2024), Evolution of rift faulting in incipient, magma-poor divergent plate boundaries: New insights from the Okavango-Makgadikgadi Rift Zone, Botswana, *Earth and* planetary science letters, 646(118957), 118,957, doi: 10.1016/j.epsl.2024.118957.
- Hamiel, Y., G. Baer, L. Kalindekafe, K. Dombola, and P. Chindandali (2012), Seismic and aseismic slip evolution and deformation associated with the 2009-2010 northern Malawi earthquake swarm, East African Rift: The 2009-2010 northern Malawi earthquake swarm, Geophysical journal international, 191(3), no–no, doi: 10.1111/j.1365-246x.2012.05673.x.
- Hellebrekers, N., A. R. Niemeijer, A. Fagereng, B. Manda, and R. L. S. Mvula (2019), Lower crustal earthquakes in the East African Rift System: Insights from frictional properties of rock samples from the Malawi rift, *Tectonophysics*, 767(228167), 228,167, doi: 10.1016/j.tecto.2019.228167.
- Hirth, G., and N. M. Beeler (2015), The role of fluid pressure on frictional behavior at the base of the seismogenic zone,

- Geology, 43(3), 223-226, doi: 10.1130/G36361.1.
- Hirth, G., and D. L. Kohlstedt (2003), Rheology of the upper mantle and the mantle wedge: A view from the experimentalists BT - geophysical monograph series, Geophysical Monograph Series, 138, 83–106.
- Hodge, M., J. Biggs, K. Goda, and W. Aspinall (2015), Assessing infrequent large earthquakes using geomorphology and geodesy: the Malawi Rift, *Natural hazards (Dordrecht, Netherlands)*, 76(3), 1781–1806, doi: 10.1007/s11069-014-1572-y.
- Hodge, M., A. Fagereng, J. Biggs, and H. Mdala (2018), Controls on early-rift geometry: New perspectives from the bilila-mtakataka fault, Malawi, Geophysical research letters, 45(9), 3896–3905, doi: 10.1029/2018gl077343.
- Hodge, M., J. Biggs, A. Fagereng, H. Mdala, L. N. J. Wedmore, and J. N. Williams (2020), Evidence from high-resolution topography for multiple earthquakes on high slip-to-length fault scarps: The Bilila-Mtakataka fault, Malawi, *Tectonics*, 39(2), e2019TC005,933, doi: 10.1029/2019tc005933.
- Hodgson, I., F. Illsley-Kemp, R. J. Gallacher, D. Keir, C. J. Ebinger, and K. Mtelela (2017), Crustal Structure at a Young Continental Rift: A Receiver Function Study From the Tanganyika Rift, *Tectonics*, 36(12), 2806–2822, doi: 10.1002/2017TC004477.
- Holmgren, J. M., M. J. Werner, K. Goda, M. Villani, V. Silva, P. Chindandali, and V. Stevens (2023), A relocated earthquake catalog and ground motion database for the southern East African rift system, Earthquake spectra: the professional journal of the Earthquake Engineering Research Institute, 39(3), 1911–1929, doi: 10.1177/87552930231173450.
- Hopper, E., J. B. Gaherty, D. J. Shillington, N. J. Accardo, A. A. Nyblade, B. K. Holtzman, C. Havlin, C. A. Scholz, P. R. N. Chindandali, R. W. Ferdinand, G. D. Mulibo, and G. Mbogoni (2020), Preferential localized thinning of lithospheric mantle in the melt-poor Malawi Rift, *Nature geoscience*, 13(8), 584–589, doi: 10.1038/s41561-020-0609-y.
- Ingleby, T., and T. J. Wright (2017), Omori-like decay of postseismic velocities following continental earthquakes: OMORI DECAY OF POSTSEISMIC VELOCITIES, Geophysical research letters, 44(7), 3119–3130, doi: 10.1002/2017gl072865.
- Jackson, J., and T. Blenkinsop (1993), The Malaŵi Earthquake of March 10, 1989: Deep faulting within the East African Rift System, *Tectonics*, 12(5), 1131–1139, doi: 10.1029/93TC01064.
- Jackson, J., and T. Blenkinsop (1997), The Bilila-Mtakataka fault in Malaŵi: An active, 100-km long, normal fault segment in thick seismogenic crust, *Tectonics*, 16(1), 137–150, doi: 10.1029/96tc02494.
- Jackson, J., D. A. N. McKENZIE, K. Priestley, and B. Emmerson (2008), New views on the structure and rheology of the lithosphere, *Journal of the Geological Society*, 165(2), 453–465, doi: 10.1144/0016-76492007-109.
- Jamtveit, B., Y. Ben-Zion, F. Renard, and H. Austrheim (2018), Earthquake-induced transformation of the lower crust, Nature, 556(7702), 487-491, doi: 10.1038/s41586-018-0045-y.
- Jess, S., D. Koehn, M. Fox, E. Enkelmann, T. Sachau, and K. Aanyu (2020), Paleogene initiation of the Western Branch of the East African Rift: The uplift history of the Rwenzori Mountains, Western Uganda, Earth

- and planetary science letters, 552(116593), 116,593, doi: 10.1016/j.epsl.2020.116593.
- Julià, J., C. J. Ammon, and A. A. Nyblade (2005), Evidence for mafic lower crust in Tanzania, East Africa, from joint inversion of receiver functions and Rayleigh wave dispersion velocities, *Geophysical journal international*, 162(2), 555–569, doi: 10.1111/j.1365-246X.2005.02685.x.
- Kachingwe, M., A. Nyblade, and J. Julià (2015), Crustal structure of Precambrian terranes in the southern African subcontinent with implications for secular variation in crustal genesis, *Geophysical journal international*, 202(1), 533–547, doi: 10.1093/gji/ggv136.
- Kendall, J.-M., and C. Lithgow-Bertelloni (2016), Why is Africa rifting?, Geological Society special publication, 420(1), 11–30, doi: 10.1144/sp420.17.
- Kinabo, B. D., J. P. Hogan, E. A. E. A. Atekwana, M. G. Abdelsalam, and M. P. Modisi (2008), Fault growth and propagation during incipient continental rifting: Insights from a combined aeromagnetic and Shuttle Radar Topography Mission digital elevation model investigation of the Okavango Rift Zone, northwest Botswana, *Tectonics*, 27(3), 1–16, doi: 10.1029/2007TC002154.
- Kirby, S. H., and A. K. Kronenberg (1987), Correction to "Rheology of the lithosphere: Selected topics", *Reviews of geophysics (Washington, D.C.: 1985)*, 25(8), 1680–1681, doi: 10.1029/rg025i008p01680.
- Kohlstedt, D. L., B. Evans, and S. J. Mackwell (1995), Strength of the lithosphere: Constraints imposed by laboratory experiments, *Journal of geophysical research*, 100(B9), 17,587-17,602, doi: 10.1029/95JB01460.
- Kolawole, F., and R. Ajala (2024), Propagating rifts: the roles of crustal damage and ascending mantle fluids, *Solid earth*, 15(7), 747–762, doi: 10.5194/se-15-747-2024.
- Kolawole, F., E. A. Atekwana, S. Malloy, D. S. Stamps, R. Grandin, M. G. Abdelsalam, K. Leseane, and E. M. Shemang (2017), Aeromagnetic, gravity, and Differential Interferometric Synthetic Aperture Radar analyses reveal the causative fault of the 3 April 2017  $M_w$  6.5 Moiyabana, Botswana, earthquake:  $M_w$ 6.5 Botswana Earthquake Fault Revealed, Geophysical research letters, 44(17), 8837–8846, doi: 10.1002/2017gl074620.
- Lavayssière, A., C. Drooff, C. Ebinger, R. Gallacher, F. Illsley-Kemp, S. J. Oliva, and D. Keir (2019), Depth Extent and Kinematics of Faulting in the Southern Tanganyika Rift, Africa, *Tectonics*, 38(3), 842–862, doi: 10.1029/2018TC005379.
- Lindenfeld, M., G. Rümpker, A. Batte, and A. Schumann (2012a), Seismicity from February 2006 to September 2007 at the Rwenzori Mountains, East African Rift: earthquake distribution, magnitudes and source mechanisms, *Solid earth*, 3(2), 251–264, doi: 10.5194/se-3-251-2012.
- Lindenfeld, M., G. Rümpker, K. Link, D. Koehn, and A. Batte (2012b), Fluid-triggered earthquake swarms in the Rwenzori region, East African Rift—Evidence for rift initiation, *Tectonophysics*, 566-567, 95–104, doi: 10.1016/j.tecto.2012.07.010.
- Lloyd, R., J. Biggs, and A. Copley (2019), The decade-long Machaze–Zinave aftershock sequence in the slowly straining Mozambique Rift, Geophysical journal international, 217(1), 504–531, doi: 10.1093/gji/ggz033.
- Macheyeki, A. S., H. Mdala, L. S. Chapola, V. J. Manhiça, J. Chisambi, P. Feitio, A. Ayele, J. Barongo, R. W. Ferdinand, G. Ogubazghi, B. Goitom, J. D. Hlatywayo, G. K. Kianji, I. Marobhe, A. Mulowezi, D. Mutamina,

- J. M. Mwano, B. Shumba, and I. Tumwikirize (2015), Active fault mapping in Karonga-Malawi after the December 19, 2009 Ms 6.2 seismic event, *Journal of African earth sciences (Oxford, England: 1994)*, 102, 233–246, doi: 10.1016/j.jafrearsci.2014.10.010.
- Mackintosh, V., B. Kohn, A. Gleadow, and K. Gallagher (2019), Long-term reactivation and morphotectonic history of the Zambezi Belt, northern Zimbabwe, revealed by multi-method thermochronometry, *Tectonophysics*, 750(vember 2018), 117–136, doi: 10.1016/j.tecto.2018.11.009.
- Mackwell, S. J., M. E. Zimmerman, and D. L. Kohlstedt (1998), High-temperature deformation of dry diabase with application to tectonics on Venus, *Journal of geophysical research*, 103(B1), 975–984, doi: 10.1029/97jb02671.
- Magistrale, H. (2001), Relative contributions of crustal temperature and composition to controlling the depth of earthquakes in Southern California, *Geophysical research letters*, 29(10), 81–87, doi: 10.1029/2001GL014375.
- Manda, B. W. C., P. A. Cawood, C. J. Spencer, T. Prave, R. Robinson, and N. M. W. Roberts (2019), Evolution of the Mozambique Belt in Malawi constrained by granitoid U-Pb, Sm-Nd and Lu-Hf isotopic data, Gondwana research: international geoscience journal, 68, 93–107, doi: 10.1016/j.gr.2018.11.004.
- Mckenzie, D., J. Jackson, and K. Priestley (2005), Thermal structure of oceanic and continental lithosphere, *Earth and planetary science letters*, 233(3-4), 337–349, doi: 10.1016/j.epsl.2005.02.005.
- Meghraoui, M., and the IGCP-601 Working Group (2016), The seismotectonic map of Africa, *Episodes*, 39(1), 9–18, doi: 10.18814/epiiugs/2016/v39i1/89232.
- Midzi, V., I. Saunders, B. Manzunzu, M. T. Kwadiba,
  V. Jele, R. Mantsha, K. T. Marimira, T. F. Mulabisana,
  O. Ntibinyane, T. Pule, G. W. Rathod, M. Sitali,
  L. Tabane, G. van Aswegen, and B. S. Zulu (2018), The
  03 April 2017 Botswana M6.5 earthquake: Preliminary
  results, Journal of African earth sciences (Oxford,
  England: 1994), 143(April 2017), 187–194, doi:
  10.1016/j.jafrearsci.2018.03.027.
- Montési, L. G. J. (2004), Controls of shear zone rheology and tectonic loading on postseismic creep: TIME DEPENDENCE OF POSTSEISMIC CREEP, Journal of geophysical research, 109(B10), doi: 10.1029/2003jb002925.
- Moorkamp, M., S. Fishwick, R. J. Walker, and A. G. Jones (2019), Geophysical evidence for crustal and mantle weak zones controlling intra-plate seismicity the 2017 Botswana earthquake sequence, *Earth and planetary science letters*, 506, 175–183, doi: 10.1016/j.epsl.2018.10.048.
- Muirhead, J. D., L. J. M. Wright, and C. A. Scholz (2019), Rift evolution in regions of low magma input in East Africa, Earth and planetary science letters, 506, 332–346, doi: 10.1016/j.epsl.2018.11.004.
- Muluneh, A. A., D. Keir, and G. Corti (2021), Thermo-rheological properties of the Ethiopian lithosphere and evidence for transient fluid induced lower crustal seismicity beneath the Ethiopian rift, *Frontiers in earth* science, 9(May), 1–11, doi: 10.3389/feart.2021.610165.
- Nair, S. K., S. S. Gao, K. H. Liu, and P. G. Silver (2006), Southern African crustal evolution and composition: Constraints from receiver function studies, *Journal of geophysical research*. Solid earth, 111(2), 1–17, doi:

#### 10.1029/2005JB003802.

- Nishimura, K., S. Uehara, and K. Mizoguchi (2019), An alternative origin of high VP/Vs anomalies in slow slip regions: Experimental constraints from the elastic wave velocity evolution of highly fractured rock, *Journal of geophysical research*. Solid earth, 124(5), 5045–5059, doi: 10.1029/2018jb016929.
- Njinju, E. A., E. A. Atekwana, D. S. Stamps, M. G. Abdelsalam, E. A. Atekwana, K. L. Mickus, S. Fishwick, F. Kolawole, T. A. Rajaonarison, and V. N. Nyalugwe (2019a), Lithospheric structure of the Malawi rift: Implications for magma-poor rifting processes, *Tectonics*, 38(11), 3835–3853, doi: 10.1029/2019tc005549.
- Njinju, E. A., F. Kolawole, E. A. Atekwana, D. S. Stamps, E. A. Atekwana, M. G. Abdelsalam, and K. L. Mickus (2019b), Terrestrial heat flow in the Malawi Rifted Zone, East Africa: Implications for tectono-thermal inheritance in continental rift basins, *Journal of volcanology* and geothermal research, 387(106656), 106,656, doi: 10.1016/j.jvolgeores.2019.07.023.
- Nyblade, A. A., and C. A. Langston (1995), East African earthquakes below 20 km depth and their implications for crustal structure, *Geophysical journal international*, 121(1), 49–62, doi: 10.1111/j.1365-246X.1995.tb03510.x.
- Nyblade, A. A., H. N. Pollack, D. L. Jones, F. Podmore, and M. Mushayandebvu (1990), Terrestrial heat flow in east and southern Africa, *Journal of geophysical research*, 95(B11), 17,371–17,384, doi: 10.1029/jb095ib11p17371.
- Paulssen, H., T. Micallef, D. R. Bouwman, E. Ruigrok, M. W. Herman, I. Fadel, M. van der Meijde, M. Kwadiba, J. Maritinkole, and O. Ntibinyane (2022), Rifting of the Kalahari craton through Botswana? New seismic evidence, Journal of geophysical research. Solid earth, 127(4), doi: 10.1029/2021jb023524.
- Petersen, T., K. Gledhill, M. Chadwick, N. H. Gale, and J. Ristau (2011), The New Zealand National Seismograph Network, Seismological research letters, 82(1), 9–20, doi: 10.1785/gssrl.82.1.9.
- Poggi, V., R. Durrheim, G. M. Tuluka, G. Weatherill, R. Gee, M. Pagani, A. Nyblade, and D. Delvaux (2017), Assessing seismic hazard of the East African Rift: a pilot study from GEM and AfricaArray, Bulletin of earthquake engineering, 15(11), 4499–4529, doi: 10.1007/s10518-017-0152-4.
- Rajaonarison, T., D. S. Stamps, and J. Naliboff (2021), Role of lithospheric buoyancy forces in driving deformation in east Africa from 3D geodynamic modeling, *Geophysical research letters*, 48(6), e2020GL090,483, doi: 10.1029/2020GL090483.
- Roberts, E. M., N. J. Stevens, P. M. O'Connor, P. H. G. M. Dirks, M. D. Gottfried, W. C. Clyde, R. A. Armstrong, A. I. S. Kemp, and S. Hemming (2012), Initiation of the western branch of the East African Rift coeval with the eastern branch, *Nature geoscience*, 5(4), 289–294, doi: 10.1038/ngeo1432.
- Roecker, S., C. Ebinger, C. Tiberi, G. Mulibo, R. Ferdinand-Wambura, K. Mtelela, G. Kianji, A. Muzuka, S. Gautier, J. Albaric, and S. Peyrat (2017), Subsurface images of the Eastern Rift, Africa, from the joint inversion of body waves, surface waves and gravity: investigating the role of fluids in early-stage continental rifting, Geophysical journal international, 210(2), 931–950, doi: 10.1093/gji/ggx220.
- Rolandone, F., R. Bürgmann, and R. M. Nadeau (2004), The evolution of the seismic-aseismic transition during the

- earthquake cycle: Constraints from the time-dependent depth distribution of aftershocks: AN EVOLVING SEISMIC-ASEISMIC TRANSITION, Geophysical research letters, 31(23), 1–4, doi: 10.1029/2004gl021379.
- Rosenberg, C. L., and M. R. Handy (2005), Experimental deformation of partially melted granite revisited: implications for the continental crust, Journal of metamorphic geology, 23(1), 19–28, doi: 10.1111/j.1525-1314.2005.00555.x.
- Rutter, E. H., and K. H. Brodie (2004), Experimental grain size-sensitive flow of hot-pressed Brazilian quartz aggregates, *Journal of Structural Geology*, 26(11), 2011–2023, doi: 10.1016/j.jsg.2004.04.006.
- Rybacki, E., and G. Dresen (2000), Dislocation and diffusion creep of synthetic anorthite aggregates, *Journal of geophysical research*. *Solid earth*, 105(B11), 26,017–26,036, doi: 10.1029/2000JB900223.
- Saria, E., E. Calais, D. S. Stamps, D. Delvaux, and C. J. H. Hartnady (2014), Present-day kinematics of the east African rift, Journal of geophysical research. Solid earth, 119(4), 3584–3600, doi: 10.1002/2013jb010901.
- Shillington, D. J., C. A. Scholz, P. R. N. Chindandali, J. B. Gaherty, N. J. Accardo, E. Onyango, C. J. Ebinger, and A. A. Nyblade (2020), Controls on rift faulting in the North Basin of the Malawi (Nyasa) rift, east Africa, *Tectonics*, 39(3), e2019TC005,633, doi: 10.1029/2019tc005633.
- Shudofsky, G. N., S. Cloetingh, S. Stein, and R. Wortel (1987), Unusually deep earthquakes in East Africa: Constraints on the thermo-mechanical structure of a continental rift system, *Geophysical research letters*, 14(7), 741–744, doi: 10.1029/gl014i007p00741.
- Sibson, R. (1982), Fault zone models, heat flow, and the depth distribution of earthquakes in the continental crust of the United States, *Bulletin of the Seismological Society of America*, 72(1), 151–163.
- Sibson, R. H. (1974), Frictional constraints on thrust, wrench and normal faults, Nature, 249(5457), 542-544, doi: 10.1038/249542a0.
- Sibson, R. H. (2000), Fluid involvement in normal faulting, *Journal of geodynamics*, 29(3-5), 469-499, doi: 10.1016/s0264-3707(99)00042-3.
- Sibson, R. H., and J. V. Rowland (2003), Stress, fluid pressure and structural permeability in seismogenic crust, North Island, New Zealand, *Geophysical journal international*, 154(2), 584–594, doi: 10.1046/j.1365-246X.2003.01965.x.
- Stamps, D. S., L. M. Flesch, E. Calais, and A. Ghosh (2014), Current kinematics and dynamics of Africa and the East African Rift System, *Journal of geophysical research*. *Solid* earth, 119(6), 5161–5186, doi: 10.1002/2013jb010717.
- Stamps, D. S., C. Kreemer, R. Fernandes, T. A. Rajaonarison, and G. Rambolamanana (2021), Redefining East African Rift System kinematics, *Geology*, 49(2), 150–155, doi: 10.1130/g47985.1.
- Stein, S., and M. Liu (2009), Long aftershock sequences within continents and implications for earthquake hazard assessment, *Nature*, 462(7269), 87–89, doi: 10.1038/nature08502.
- Stevens, V. L., R. A. Sloan, P. R. Chindandali, L. N. J. Wedmore, G. W. Salomon, and R. A. Muir (2021), The Entire Crust can be Seismogenic: Evidence from Southern Malawi, *Tectonics*, 40(6), doi: 10.1029/2020tc006654.
- Sun, M., S. S. Gao, K. H. Liu, K. Mickus, X. Fu, and Y. Yu (2021), Receiver function investigation of crustal structure

- in the Malawi and Luangwa rift zones and adjacent areas, Gondwana research: international geoscience journal, 89, 168–176, doi: 10.1016/j.gr.2020.08.015.
- Tugume, F., A. Nyblade, and J. Julià (2012), Moho depths and Poisson's ratios of Precambrian crust in East Africa: Evidence for similarities in Archean and Proterozoic crustal structure, *Earth and planetary science letters*, 355-356, 73-81, doi: 10.1016/j.epsl.2012.08.041.
- Tulley, C. J., A. Fagereng, and K. Ujiie (2020), Hydrous oceanic crust hosts megathrust creep at low shear stresses, *Science advances*, 6(22), eaba1529, doi: 10.1126/sciadv.aba1529.
- Von Herzen, R. P., and V. Vacquier (1967), Terrestrial heat flow in Lake Malawi, Africa, Journal of geophysical research, 72(16), 4221–4226, doi: 10.1029/JZ072i016p04221.
- Wanke, H. (2005), The Namibian Eiseb Graben as an extension of the East African Rift: evidence from Landsat TM 5 imagery, Suid-Afrikaanse tydskrif vir geologie [South African journal of geology], 108(4), 541–546, doi: 10.2113/108.4.541.
- Wedmore, L. N. J., J. Biggs, J. N. Williams, A. Fagereng, Z. Dulanya, F. Mphepo, and H. Mdala (2020a), Active fault scarps in southern Malawi and their implications for the distribution of strain in incipient continental rifts, *Tectonics*, 39(3), e2019TC005,834, doi: 10.1029/2019tc005834.
- Wedmore, L. N. J., J. N. Williams, J. Biggs, A. Fagereng, F. Mphepo, Z. Dulanya, J. Willoughby, H. Mdala, and B. A. Adams (2020b), Structural inheritance and border fault reactivation during active early-stage rifting along the Thyolo fault, Malawi, *Journal of structural geology*, 139(104097), 104,097, doi: 10.1016/j.jsg.2020.104097.
- Wedmore, L. N. J., J. Biggs, M. Floyd, A. Fagereng, H. Mdala, P. Chindandali, J. N. Williams, and F. Mphepo (2021), Geodetic constraints on cratonic microplates and broad strain during rifting of thick southern African lithosphere, Geophysical research letters, 48(17), doi: 10.1029/2021gl093785.
- Wedmore, L. N. J., T. Turner, J. Biggs, J. N. Williams, H. M. Sichingabula, C. Kabumbu, and K. Banda (2022), The Luangwa Rift Active Fault Database and fault reactivation along the southwestern branch of the East African Rift, *Solid earth*, 13(11), 1731–1753, doi: 10.5194/se-13-1731-2022.
- Wedmore, L. N. J., D. Evans, J. N. Williams, J. Biggs, A. Fagereng, P. Mawejje, F. Tugume, T. Blenkinsop, and D. E. J. Hobley (2024), The early onset of magmatic rift faulting in the Edward-George Rift, Uganda, *Earth* and planetary science letters, 638(118762), 118,762, doi: 10.1016/j.epsl.2024.118762.
- Wilks, K. R., and N. L. Carter (1990), Rheology of some continental lower crustal rocks, *Tectonophysics*, 182(1-2), 57–77, doi: 10.1016/0040-1951(90)90342-6.
- Williams, J. N., A. Fagereng, L. N. J. Wedmore, J. Biggs, F. Mphepo, Z. Dulanya, H. Mdala, and T. Blenkinsop (2019), How Do Variably Striking Faults Reactivate During Rifting? Insights From Southern Malawi, *Geochemistry, geophysics, geosystems:* G(3), 20(7), 3588–3607, doi: 10.1029/2019GC008219.
- Williams, J. N., L. N. J. Wedmore, C. A. Scholz, F. Kolawole, L. J. M. Wright, D. J. Shillington, A. Fagereng, J. Biggs, H. Mdala, Z. Dulanya, F. Mphepo, P. R. N. Chindandali, and M. J. Werner (2022a), The Malawi active fault

- An onshore-offshore database for regional assessment of seismic hazard and tectonic evolution, Geochemistry, geophysics, geosystems: G(3), 23(5),e2022GC010,425, doi: 10.1029/2022gc010425.
- Williams, J. N., A. Fagereng, L. N. J. Wedmore, J. Biggs, H. Mdala, F. Mphepo, and M. Hodge (2022b), Low dissipation of earthquake energy where a fault follows pre-existing weaknesses: Field and microstructural observations of Malawi's bilila-mtakataka fault, Geophysical research letters, 49(8), e2021GL095,286, doi: 10.1029/2021gl095286.
- Williams, J. N., L. N. J. Wedmore, A. Fagereng, M. J. Werner, H. Mdala, D. J. Shillington, C. A. Scholz, F. Kolawole, L. J. M. Wright, J. Biggs, Z. Dulanya, F. Mphepo, and P. Chindandali (2022c), Geologic and geodetic constraints on the magnitude and frequency of earthquakes along Malawi's active faults: the Malawi Seismogenic Source Model (MSSM), Natural hazards and earth system sciences, 22(11), 3607-3639, doi: 10.5194/nhess-22-3607-2022.
- Williams, J. N., M. J. Werner, K. Goda, L. N. J. Wedmore, R. De Risi, J. Biggs, H. Mdala, Z. Dulanya, A. Fagereng, F. Mphepo, and P. Chindandali (2023), Fault-based probabilistic seismic hazard analysis in regions with low strain rates and a thick seismogenic layer: a case study from Malawi, Geophysical journal international, 233(3), 2172–2207, doi: 10.1093/gji/ggad060.
- Williams, J. N., D. Eberhart-Phillips, S. Bourguignon, M. W. Stirling, and W. Oliver (2025), Deep and clustered microseismicity at the edge of southern new zealand's

- transpressive plate boundary, Journal of geophysical research. Solid earth, 130(5), e2024JB030,371, doi: 10.1029/2024jb030371.
- Wintsch, R. P., R. Christoffersen, and A. K. Kronenberg (1995), Fluid-rock reaction weakening of fault zones, Journal of geophysical research, 100(B7), 13,021–13,032, doi: 10.1029/94jb02622.
- Wood, D. A., H. J. Zal, C. A. Scholz, C. J. Ebinger, and I. Nizere (2017), Evolution of the Kivu Rift, East Africa: interplay among tectonics, sedimentation and magmatism, Basin research, 29, 175-188, doi: 10.1111/bre.12143.
- Wright, T., J. Elliott, H. Wang, and I. Ryder (2013), Earthquake cycle deformation and the Moho: Implications for the rheology of continental lithosphere, Tectonophysics, 609, 504–523, doi: 10.1016/J.TECTO.2013.07.029.
- Yang, Z., and W.-P. Chen (2010), Earthquakes along the East African Rift System: A multiscale, system-wide perspective, Journal of geophysical research, 115(B12), doi: 10.1029/2009jb006779.
- Yu, Y., K. H. Liu, C. A. Reed, M. Moidaki, K. Mickus, E. A. Atekwana, and S. S. Gao (2015), A joint receiver function and gravity study of crustal structure beneath the incipient Okavango Rift, Botswana, Geophysical research letters, 42(20), 8398–8405, doi: 10.1002/2015gl065811.
- Zertani, S., M. Thielmann, and L. Menegon (2025), Lower-crustal earthquakes: Strain rate controls the magnitude and rate of stress amplification in rigid blocks, Geophysical research letters, 52(7), doi: 10.1029/2024 gl1114350.